



DEPARTAMENT DE MATEMÀTICA APLICADA III  
UNIVERSITAT POLITÈCNICA DE CATALUNYA

A REAL-TIME WAVE MONITORING APPLICATION TOOL  
FOR WAVE AGITATION IN HARBOURS

MASTER IN CIVIL ENGINEERING

*Author:*

Jon Goñi

*Supervisor:*

Antonio Huerta

*External supervisor:*

David Modesto

Barcelona

October, 2015

## Abstract

Numerical simulations of the wave agitation problem in elliptic harbour models are limited by the high computational cost of the actual models requiring a multitude of values of the incoming wave parameters. These simulations often evaluate a single incident wave to obtain the wave height inside the harbour area.

This thesis aims to overcome this obstacle by considering several outputs of interest for the practices of coastal engineering and harbour design, and their implementation in an integrated environment capable of real-time wave monitoring. Additional outputs such as protective indexes and wave potential energy are given by any value of the incoming wave parameters (frequency and direction), providing any problem solution can be obtained at a negligible computational cost with a wide range of possibilities for user interaction.

The proposed real-time framework is integrated in a graphical user interface, developed in a MATLAB<sup>©</sup> environment that allows a deep interaction with the wave agitation solution to obtain several outputs of interest for the assessment of harbour operability in real-time. The interface also models the effects of the wave input parameters on a user-specified area, allowing the direct and fast identification of the incoming wave periods and directions that, for instance, compromise port operations, or cause a resonant response on the geometry. Additionally, solutions obtained for individualized sets of queries can be combined with spectral functions to form combinations of interest to the user.

The real-time evaluation is made possible by the use of a reduced order model approach with which a generalized solution for any incoming wave parameter is computed. Other techniques used in previous works of finite elements in elliptic harbour models are also used, including the use of perfectly matched layers to truncate the exterior domain, and the spacial discretization using high-order finite elements to accurately describe the obtained solution field in the whole computational domain.

Finally, a numerical example is for the real wave agitation in the Mataro harbour is used to demonstrate the capabilities of the proposed tool.



# Contents

<b>List of Figures</b>	<b>v</b>
<b>1 Introduction</b>	<b>1</b>
1.1 Motivation . . . . .	1
1.2 The harbour wave agitation problem . . . . .	2
1.3 Thesis objectives . . . . .	3
<b>2 Elliptic harbour models</b>	<b>5</b>
2.1 Elliptic harbour models . . . . .	5
2.1.1 Mild-Slope Equation . . . . .	8
2.1.2 Problem statement . . . . .	9
2.2 Real-time wave monitoring using reduced order modelling . . . . .	11
2.2.1 The generalized solution . . . . .	12
2.2.2 Proper Generalized Decomposition . . . . .	13
<b>3 The real-time application tool</b>	<b>17</b>
3.1 Outputs of interest for harbour models aimed towards coastal engineering .	17
3.1.1 Real-time solutions for any particularized mesh node . . . . .	18
3.1.2 Wave Height . . . . .	18
3.1.3 Limit Height . . . . .	19
3.1.4 Spectral distributions . . . . .	19
3.1.5 Protective Index . . . . .	21
3.1.6 Wave Potential . . . . .	21
3.1.7 Resonance studies . . . . .	22
3.1.8 Spatial solution . . . . .	24
3.2 Implementation and GUI design . . . . .	25
3.2.1 Description of the file system . . . . .	25
3.2.2 Data and handles structures . . . . .	28
3.2.3 Layout and elements description . . . . .	32

<b>4 Numerical applications</b>	<b>39</b>
4.1 Geometries, bathymetries and incident wave data . . . . .	39
4.2 A realistic application: Mataro harbour . . . . .	44
<b>5 Discussion</b>	<b>55</b>
5.1 Summary and conclusions . . . . .	55
5.2 Future work . . . . .	56
<b>Bibliography</b>	<b>57</b>

# List of Figures

1.1	Oyster Wave Energy capturing device	2
2.1	Water particle elliptic trajectories on propagating wave	6
2.2	Stages of an incoming wave incidence on a perfectly reflective boundary	7
2.3	Wave diffraction	7
2.4	Sketch of the PML regions in the harbour of Mataro	10
3.1	GUI folder structure	25
3.2	GUI tools	26
3.3	Graphical User Interface layout	32
3.4	Port Selection Map: The selected port's information is shown in the textbox prior to the loading sequence	32
3.5	PGD information panel	33
3.6	Scalar field selection tabs for the main plot axes	33
3.7	Scalar field data visualization options panel	34
3.8	Coordinate panel	34
3.9	Output panel	35
3.10	Incoming wave panel	36
3.11	User function selector	36
3.12	Example of wave height distribution plots along the incoming frequency and direction parametric coordinates.	37
3.13	Spatial point selector for user-specified region	38
4.1	Geometric contour of the Pasaia harbour, with the PML included.	40
4.2	High-order Finite Element discretization of the Pasaia harbour.	41
4.3	Bathymetry drawing for the Pasaia harbour. Plan provided by Pasajes Port Authority	42
4.4	Interpolated bottom surface in the Pasaia harbour	43
4.5	Input parameters validation results	44
4.6	Main figure with the Port of Mataro loaded	45

4.7	Scalar output variable field surfaces . . . . .	46
4.8	Results of 3D surface rotation testing . . . . .	47
4.9	Main Plot visibility layer options . . . . .	48
4.10	Boundary PML region dimensions on background image . . . . .	48
4.11	Examples of plot visualization transparency combinations . . . . .	49
4.12	Comparison between Mean and Weighted Average combined solutions . . . . .	50
4.13	Parametric distribution interactive feature testing results . . . . .	51
4.14	Area maximum, average and minimum selections and distributions testing results . . . . .	53
4.15	Limit surface test results . . . . .	54

# Chapter 1

## Introduction

### 1.1 Motivation

Numerical simulations of the harbour wave agitation problem have been widely performed in the last decades, see for instance Berkhoff (1972); Bettess (1977); Berkhoff et al. (1982); Kirby (1984); Kofoed-Hansen et al. (2005). Coastal infrastructure design and harbour logistic operations are highly dependant on the wave agitation induced by the incoming sea state, as shown by González-Marco et al. (2008); Demirbilek et al. (1996); Adytia et al. (2012). The resulting wave field inside the port is affected by several factors such as geometry or the marine climate. An adverse wave agitation can compromise naval operations and cause collisions that can damage both vessels and harbour structures. Providing coastal engineers with the capacity to assess the harbour wave agitation for any incoming wave carries a high interest, as these data can also be used to determine several key wave parameters. These parameters, in turn, can be used to forecast and hindcast the long term ocean climate and thus have great significance on the construction and management of offshore infrastructure, development of port and harbour structures, and naval operations, see Muir and El-Shaarawi (1986); Rodriguez et al. (2002); Soares and Carvalho (2003).

Previous work on the field of numerical wave monitoring has mainly focused on the measurement of the wave height field. The first prediction models were developed during the Second World War with military applications, see Cox and Cardone (2002). These models were, however, very limited in their approach and accuracy, aiming to predict the propagating wave height. Later advancements relying on the increased computational processing power include many different approaches to the wave height prediction, often including physical effects such as ocean bottom drag, superficial energy dissipation (wave breaking) or the analysis of long waves for resonance studies. These approaches, however, still require an extensive computational power to generate a solution for each query, which makes them unsuitable for several applications of coastal engineering. This thesis aims

to provide an environment in which the real-time computation of several outputs of interest for the practices of harbour management and ocean engineering are integrated and obtained at a negligible computational cost.

There are several applications for the many parameters that can be obtained from the harbour wave agitation problem, and many of them are very promising in several areas of increased importance. For instance, critical incoming wave frequencies and directions can be identified to determine which port operations are not recommended by current standards for the predicted sea state to reduce economic losses to a minimum, as shown by Srokosz and Challenor (1987); Masson and Chandler (1993). The potential energy of a wave is another example of an easy-to-obtain indicator of the theoretical renewable energetic output that could be extracted from it as seen in Mørk et al. (2010), an important magnitude when considering the ever-increasing interest in alternative energy sources, see Clément et al. (2002); Thomas and Dwarakish (2015).



Figure 1.1: Oyster Wave Energy capturing device

## 1.2 The harbour wave agitation problem

The wave agitation problem has been extensively modelled since the 1960s to describe the propagation of water waves along the horizontal plane, see Liu and Losada (2002) for a historical perspective. It is based on the Navier-Stokes equations, and the propagation is shaped by the effects of diffraction, reflection and refraction. Due to the dependence of the first two phenomena on physical obstacles whose properties can be idealized as parameters on the wave field, and the possibility to integrate the depth dependence of refraction in the horizontal domain, the problem can be fully idealized in a 2D domain. As seen in Liu and Losada (2002), several models exist nowadays to model the nearshore transformations produced by these phenomena. Out of them, the most used ones are based either on the Boussinesq or Mild-Slope Equations, with the later one being more

adequate for the applications on this thesis due to its higher flexibility on depth range and minor computational cost for large scale problems, see LI et al. (2005) for details.

In 1972 Berkhoff derived the Mild-Slope Equation as seen in Berkhoff (1972), which takes into account the combined effects of reflection, refraction and diffraction while integrating the depth variable by means of the dispersion relation. It has since been used extensively to model bidimensional wave propagation models in mild slopes ( $< 1/3$ ) of sea bottom with many different applications, from computationally expensive second-order models that take into account wave breaking and bottom friction, to reduced-cost models by means of parabolic approximations that neglect the directional second order derivatives. It achieves a higher accuracy when the area to be modelled is relatively small (see LI et al. (2005)), and its versatility for different depths makes it ideal for the uses of the software developed in this thesis, due to the irregular bathymetries modelled in harbours.

The applications presented in this thesis require a relatively low computational cost for large scale problems, and thus the linear elliptic mild-slope solution is adopted. Additionally, artificial absorbing perfectly matched layers are used as the non-reflecting boundary condition for this problem, in order to achieve reduced computational domains.

### 1.3 Thesis objectives

This thesis aims to create an environment in which several outputs related to the wave height variable are integrated and obtained at a low computational cost. With this main goal in mind, the following secondary objectives are fulfilled:

- **Understand and implement the techniques used for the reduced order approach of the elliptic wave agitation model:** Chapter 2 gives an overview of the previous work on reduced-cost elliptic harbour models with a brief explanation of the techniques used to obtain solutions in real-time.
- **Define a set of outputs of interest that can be obtained and implemented on the current model:** The first part of Chapter 3 describes the findings on the suitable outputs of interest to the fields of coastal engineering and harbour management.
- **Create a Graphical User Interface via MATLAB<sup>©</sup> in which the outputs are integrated with the maximum degree of user-friendliness:** The second part of Chapter 3 discusses the development of the environment in which the obtained applications are integrated, and the possibilities of interaction.
- **Idealize and obtain the generalized solution of a real-life example in which the software can be tested:** Chapter 4 introduces realistic applications of harbour wave agitation problems in which the tool can be tested. The Pasaia harbour

geometry, bathymetry and histograms are used to obtain a set of data with which a generalized solution can be obtained.

- **Demonstrate the tool's capabilities in a realistic example:** The final section of Chapter 4 displays a set of the possible applications of the tool using the real geometry of the Mataro harbour.

Finally, the obtained results and completed objectives are discussed in Chapter 5.

# Chapter 2

## Elliptic harbour models

The main goal of this thesis is to develop a MATLAB<sup>©</sup> software demonstration tool that can effectively model several outputs of interest for the wave agitation problem in real-time. This chapter presents the problem statement for an elliptic harbour model, and also gives an overview of the numerical technique used to drastically decrease the computational demand needed to obtain the desired results. In order to do that, the general principle of domain discretization using high-order finite elements is outlined, while the final part focuses on the approach taken to obtain a solution that makes possible the real-time monitoring of harbour wave agitation. See Modesto (2014) for a more detailed explanation.

### 2.1 Elliptic harbour models

The wave generation and propagation processes are shaped by two interactions that take place on different physical domains:

Initially, the interaction between the sea-atmosphere surface and several phenomena including wind, earthquakes or gravitational forces is the cause of wave generation. These forces transmit energy to the water body, generating mechanical energy that is propagated following the principles of the Wave Theory.

The second stage in the process is the transfer of wave energy to the physical obstacles encountered on the propagation stage. These boundaries are divided into two groups: Those located in the horizontal plane, such as breakwaters, vessels, offshore constructions or natural contours, and the vertical interaction with the sea bed. Other aspects like terrain topography or wind intensity and direction can also have an effect on the propagating wave, but if non-linear effects such as wave breaking, sea bottom drag force or underwater currents are not considered, the generation and transportation of wave energy can be directly related to the wave height. The physical problem that is described on this thesis only focuses on the propagating phase, considering the effects of the generating forces only

through the input parameters, direction and frequency, as seen in the work by Modesto (2014).

In Linear Wave Theory, the interactions with the aforementioned physical obstacles are shaped by the reflection, refraction and diffraction phenomena, neglecting the effects of nonlinearities such as sea bed drag or wave breaking, as shown by Berkhoff et al. (1982)

The refraction phenomenon occurs when the wavefronts approach shallow waters. The particles that compose a wave follow an elliptic movement as it propagates. When the depth of the water body is not enough to prevent interaction between the water particles and the sea bed on the lower points of these trajectories, friction is created between the wave and the bottom surface, decelerating the advancing wavefront. Thus, different waves generated by the same source may exhibit varying velocities when propagating along a non-uniform bathymetry. The consequence of this behaviour is that parts of the same wave that are travelling along a shallow area will advance at a slower speed than the deeper fronts, originating the rotational effect that defines the phenomenon. More details are given by Massel (1993); Tsay and Liu (1983).

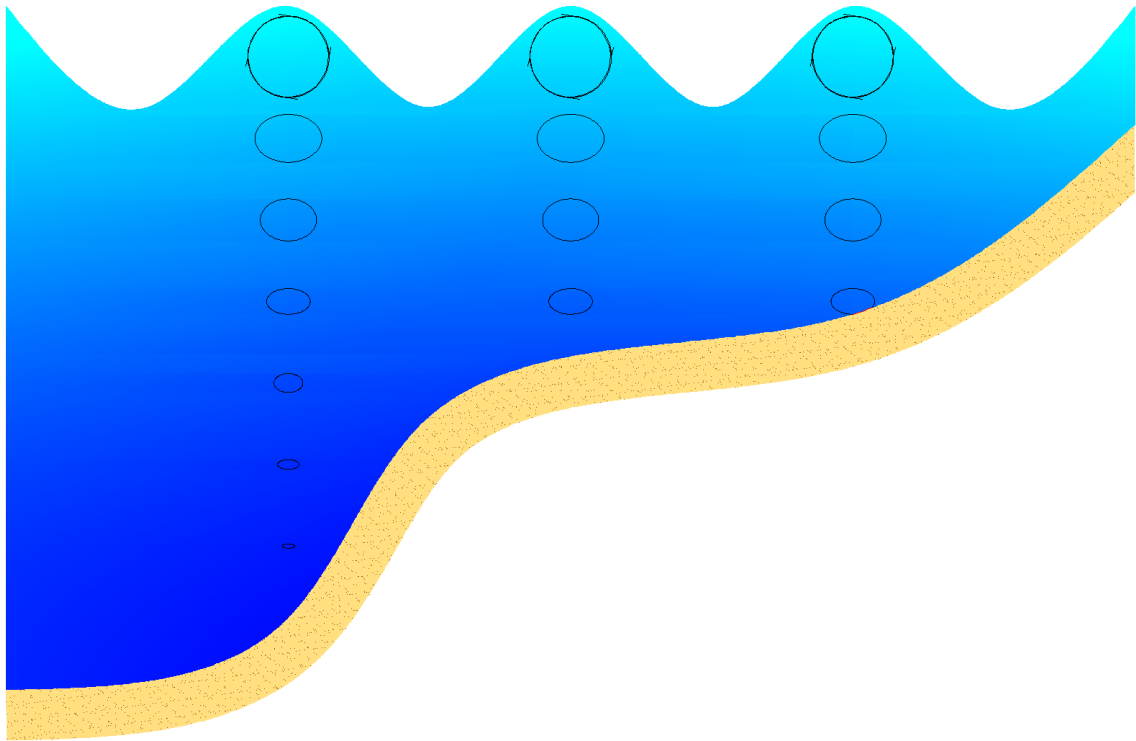
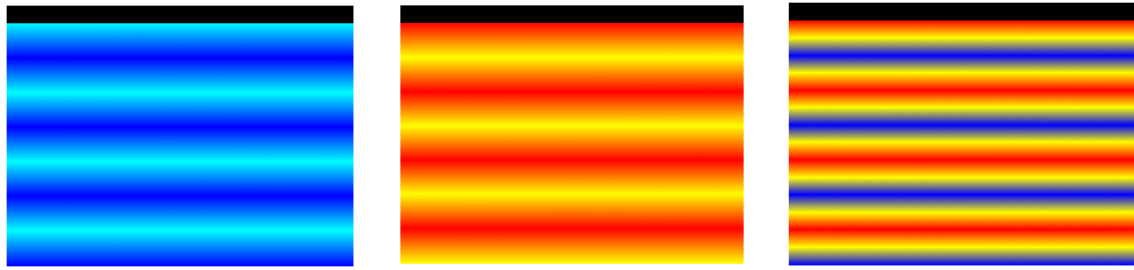


Figure 2.1: Water particle elliptic trajectories on propagating wave

Reflection and diffraction occur when a propagating wave hits a physical obstacle. If the contour either partially or totally reflects the incident wave reflection occurs. Factors that determine this behaviour include the slope of the physical obstacle, its rugosity and permeability. Typically this phenomenon is more visible on contours whose dimensions

exceed the incoming wavelength. If, on the contrary, the dimensions of the physical ob-



(a) Incident wave advancing on solid contour      (b) Reflected wave returning from solid contour      (c) Incident and reflected wave overlapping area

Figure 2.2: Stages of an incoming wave incidence on a perfectly reflective boundary

stacle are smaller or similar to the wavelength, the incoming wave's energy is transferred following the high energy gradient located perpendicular to the propagating direction, causing the diffraction of the wavefront.

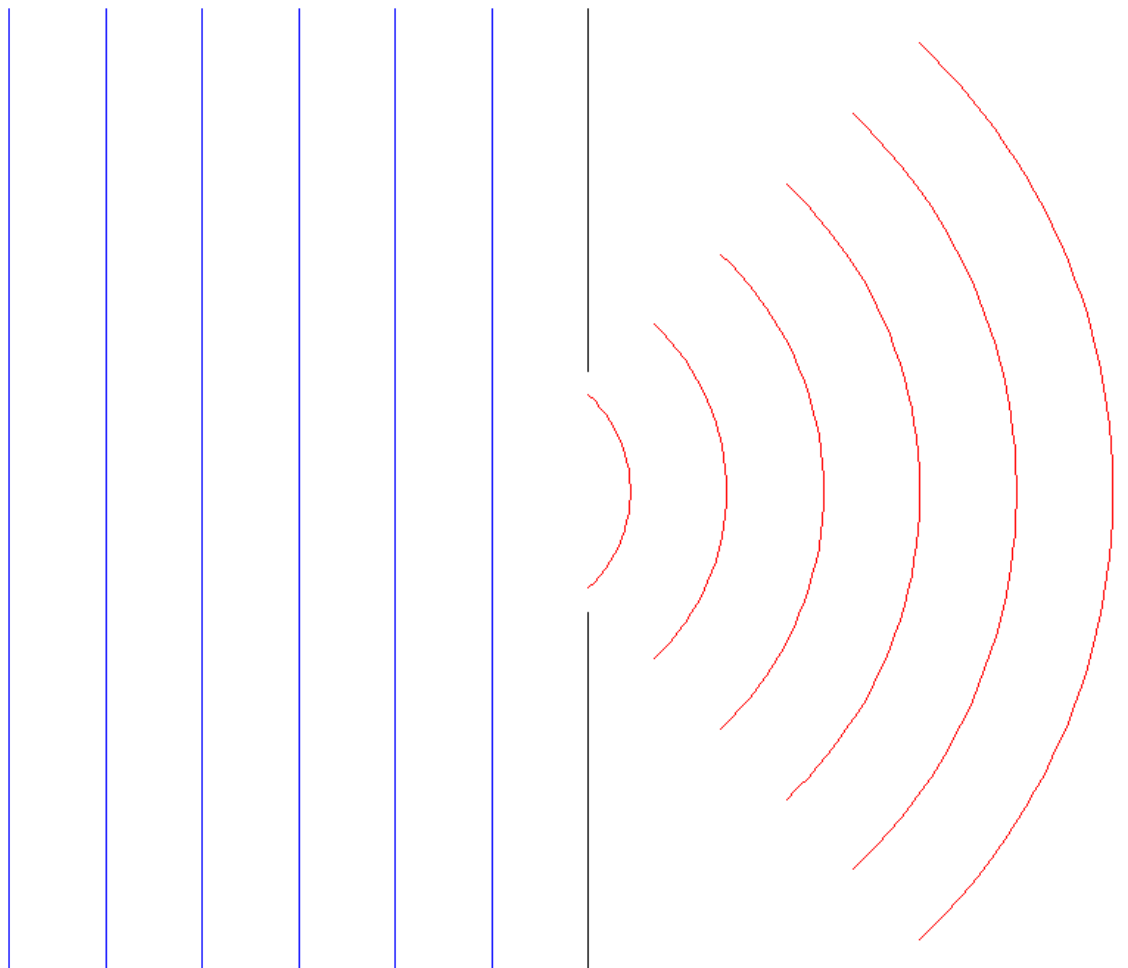


Figure 2.3: Wave diffraction

The case study of this thesis focuses on the linear phenomena that shape wave propagation over a smooth non-uniform bathymetry, which can be accurately modelled using the Mild-Slope Equation.

### 2.1.1 Mild-Slope Equation

In coastal engineering, the Mild-Slope Equation is one of the most widely used models for studies dealing with harbour wave propagation. It can evaluate in a practical and efficient manner the processes that shape wave transformation over a non-uniform bathymetry at early stages of design. Models based on the MSE can solve both linear and nonlinear processes that take place during the propagation of the wavefront towards the shoreline on a bidimensional domain. In this thesis, the linear elliptic form of the MSE in the frequencial domain gives the free surface elevation  $u(x, y) \in \mathbb{C}$  of the monochromatic waves as they propagate along a semi-infinite domain  $\Omega_{\text{inf}} \subset \mathbb{R}^2$  by the following expression:

$$\nabla \cdot (c c_g \nabla u) + k^2 c c_g u = 0 \text{ in } \Omega_{\infty} \quad (2.1)$$

Where:

$\nabla \cdot = (\frac{\partial}{\partial x}, \frac{\partial}{\partial y})$ ,  $x$  and  $y$  are the spatial coordinates.

$k(x, y) \in \mathbb{R}$  is the wavenumber.

$c = \omega/k \in \mathbb{R}$  is the phase velocity.

$\omega \in I_{\omega} \subset \mathbb{R}$  is the angular frequency of the monochromatic incident wave.

$c_g = \partial \omega / \partial k \in \mathbb{R}$  is the group velocity.

The wavenumber  $k(x, y)$  is governed by the global dispersion relation derived from the Airy Wave Theory:

$$\omega^2 = gk \tanh(kh) \quad (2.2)$$

The Mild-Slope Equation requires a full physical truncation on the boundary of the semi-infinite domain. At the shoreward, the physical obstacles conform the following boundary condition:

$$\mathbf{n} \cdot c c_g \nabla \cdot u - ik c c_g \alpha u = 0 \text{ on } \Gamma_R \quad (2.3)$$

Where:

$i = \sqrt{-1}$  is the imaginary unit.

$\mathbf{n}$  is the outer unit normal to the boundary.

$\alpha \in [0, 1]$  is the absorption/reflection coefficient of the boundary, equal to 0 in perfectly reflecting boundaries and 1 in fully absorbent ones.

At the offshore infinite domain, on the other hand, a first-order Sommerfeld radiation condition is required, which imposes that the scattered wave only has geometrical diffusion:

$$\lim_{r \rightarrow \infty} \sqrt{r} \left( \frac{\partial}{\partial r} \right) (u - u_0) = 0 \quad (2.4)$$

Where:

$r$  is the radial direction.

$u_0(x, y) \in \mathbb{C}$  is the imposed incident wave.

$u - u_0$  is the scattered wave.

As it was previously mentioned, (2.1.1) requires a spatial truncation to use a bounded computational domain and reproduce the Sommerfeld radiation effect on the artificial boundary. The use of *Perfectly Matched Layers* is the method adopted in this thesis to fulfil this requirement.

### 2.1.2 Problem statement

Truncation of the offshore infinite domain is mandatory to satisfy the existing Sommerfeld boundary condition in the wave propagation problem. This aspect has often been the source of bottlenecks in the computational models that try to solve the harbour wave agitation problem in an efficient manner, raising the need for a robust algorithm capable of accurate reproduction of the unbounded boundary conditions to reduce the computational requirements of the model to a minimum. The basic principle of the PML is that it completely absorbs any incoming wave from the non-PML domain, allowing to truncate the model without interfering on the interior solution, regardless of the incoming wave direction.

The aim of the application of the PML is to truncate the currently unbounded  $\Omega_\infty$  domain to obtain a finite interior area  $\Omega_{\text{int}}$  surrounded by a Perfectly Matched Layer  $\Omega_{\text{PML}}$ . Through the consideration approximations such as in Panchang et al. (2000), the absorbing layer can be divided into four subdomains  $\Omega_{\text{PML}} = \Omega_{\text{PML}}^{Lx} \cup \Omega_{\text{PML}}^{Rx} \cup \Omega_{\text{PML}}^y \cup \Omega_{\text{PML}}^{x,y}$  in accordance with the bathymetry simplifications adopted in each one:

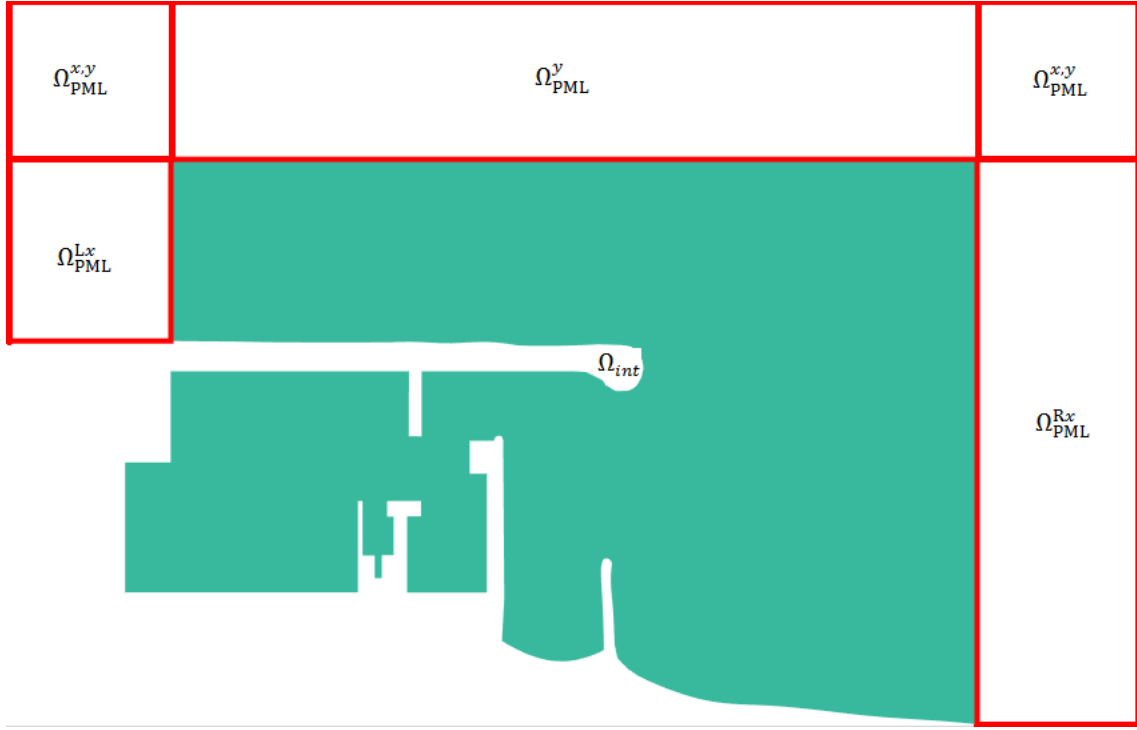


Figure 2.4: Sketch of the PML regions in the harbour of Mataro

$$h(x, y) = \begin{cases} h^L(y) & \text{if } (x, y) \in \Omega_{\text{PML}}^{Lx} \\ h^R(y) & \text{if } (x, y) \in \Omega_{\text{PML}}^{Rx} \\ h_0 & \text{if } (x, y) \in \Omega_{\text{PML}}^y \cup \Omega_{\text{PML}}^{x,y} \end{cases} \quad (2.5)$$

The adopted gradient decomposition means that the bathymetry only varies along the  $y$  direction on the  $\Omega_{\text{PML}}^{Lx}$  and  $\Omega_{\text{PML}}^{Rx}$  domains, while the  $h_0$  depth is adopted as the far-field bathymetry on the  $\Omega_{\text{PML}}^y$  and  $\Omega_{\text{PML}}^{x,y}$  domains.

Once all of the hypotheses outlined in (2.1.2) are adopted, the problem statement for the frequential form of the MSE is particularized for the PML as:

$$\nabla(c c_g \mathbf{P} \nabla \cdot u) + k^2 c c_g s_x s_y u = f(x, y) \quad \text{in } \Omega \quad (2.6a)$$

$$\mathbf{n} \cdot (c c_g \mathbf{P} \nabla \cdot u) - ik c c_g \alpha u = 0 \quad \text{on } \Gamma_R \quad (2.6b)$$

$$\mathbf{n} \cdot (c c_g \mathbf{P} \nabla \cdot u) - ik c c_g u = \mathbf{n} \cdot (c c_g \mathbf{P} \nabla \cdot u_0) - ik c c_g u_0 \quad \text{on } \Gamma_{\text{PML}} \quad (2.6c)$$

Where:

$$f = \begin{cases} 0 & \text{if } (x, y) \in \Omega_{\text{int}} \\ \nabla \cdot (c c_g \mathbf{P} \nabla \cdot u_0) + k^2 c c_g s_x s_y u_0 & \text{if } (x, y) \in \Omega_{\text{PML}} \end{cases} \quad (2.7)$$

$$\mathbf{P} = \begin{pmatrix} s_y/s_x & 0 \\ 0 & s_x/s_y \end{pmatrix} \quad (2.8)$$

Here,  $f$  is the non-homogeneous source term defined in (2.6), with the physical meaning of (2.1.2) being that  $f$  only absorbs scattered waves in the PML region. The diagonal anisotropy matrix (2.8), on the other hand, defines the absorption in the PML,  $s_x = 1 + \sigma_x/\omega$  and  $s_y = 1 + \sigma_y/\omega$  being the absorption parameters in Cartesian directions. Consequently, the absorbing functions  $\sigma_x(x) \geq 0$  and  $\sigma_y(y) \geq 0$  are zero in  $\Omega_{\text{int}}$ . Equation (2.6c) is the discrete form of the non-reflecting boundary condition introduced in (2.1.1).

Special care has to be taken when designing a PML area, as several conditions have to be met in order to accurately mimic the original semi-infinite domain:

- $\nabla \cdot (c c_g \nabla u) + k^2 c c_g u_0 = 0$  in the PML region.
- Absorption coefficients must be constant along the  $x$  direction in the  $\Omega_{\text{PML}}^{Lx} \cup \Omega_{\text{PML}}^{Rx} \cup \Omega_{\text{PML}}^{x,y}$  subdomains.
- Absorption coefficients must be constant along the  $y$  direction in the  $\Omega_{\text{PML}}^y \cup \Omega_{\text{PML}}^{x,y}$  subdomains.

These conditions are in accordance with the bathymetry restrictions mentioned in (2.1.2). Additionally, in consistence with the problem definition, continuity requirements thorough the full domain are placed on the solution, its first and second derivatives. Previous studies like the one by Michler et al. (2007) have shown that the thickness of the PML domain has to be at least equal to 1.5 times the maximum wavelength to be modelled in the simulation.

## 2.2 Real-time wave monitoring using reduced order modelling

Real-time assessments of the outputs of interest for the practices of coastal engineering and harbour management require a drastic reduction of the calculation time that is currently needed to obtain the MSE solution. This chapter gives an overview of the existing method to overcome the computational limitation, based on an *a priori* reduced order model strategy presented by Modesto (2014) to obtain the solutions for multiple queries efficiently.

### 2.2.1 The generalized solution

The first stage aims to obtain a generalized solution of the MSE in (2.6) for a 4D domain made up by the spatial dimensions  $(x, y)$  and two additional parametric dimensions, frequency  $\omega$  and incoming wave direction  $\theta$ . This would allow to evaluate in real-time any tentative scattering situation from the resulting generalized domain, which is discussed in (2.2.2).

Thus, the  $u(x, y)$  solution for the problem statement in (2.6) is generalized for a range of incoming wave direction  $\theta \in I_\theta$  and angular frequency  $\omega \in I_\omega$ , resulting in the  $u(x, y, \omega, \theta)$  surface elevation. The variational problem equivalent to (2.6) requires finding  $u$  for all  $\delta u$  in the selected appropriate functional space such that:

$$A(u, \delta u) = L(\delta u) \quad (2.9a)$$

The non-hermitian bilinear form  $A(\cdot, \cdot)$  and the linear form  $L(\cdot)$  are defined by:

$$A(u, \delta u) = \int_{I_\theta} \int_{I_\omega} a(u, \delta u; \omega) d\omega d\theta \quad \text{and} \quad L(\delta u) = \int_{I_\theta} \int_{I_\omega} \ell(\delta u; \omega, \theta) d\omega d\theta \quad (2.9b)$$

With  $a(\cdot, \cdot; \omega)$  bilinear and continuous form and  $\ell(\cdot; \omega, \theta)$  linear bounded functional for all parameters  $(\omega, \theta) \in I_\omega \times I_\theta$ . They are the classical Helmholtz spatial weak forms with the parameter dependence explicitly indicated, that is:

$$\begin{aligned} a(u, \delta u; \omega) &= (k^2 c c_g s_x s_y u, \delta u)_\Omega - (c c_g \mathbf{P} \nabla u, \nabla \delta u)_\Omega \\ &\quad + i\alpha \langle k c c_g u, \delta u \rangle_{\Gamma_R} + i \langle k c c_g u, \delta u \rangle_{\Gamma_{\text{pml}}} \end{aligned} \quad (2.10a)$$

and

$$\ell(\delta u; \omega, \theta) = (s, \delta u)_\Omega + \langle \mathbf{n} \cdot (c c_g \mathbf{P} \nabla u_0) - ik c c_g u_0, \delta u \rangle_{\Gamma_{\text{pml}}} \quad (2.10b)$$

Where:

$(\cdot, \cdot)_D$  denotes the  $\mathcal{L}^2$  scalar product (for complex functions) in any domain  $D$ .

$\langle \cdot, \cdot \rangle_B$  denotes the  $\mathcal{L}^2$  scalar product of the traces over  $B$ .

Increasing the number of dimensions on the solution carries an exponential growth in computational cost. The aim of the reduced order method explained next is to reduce the associated costs to a level comparable to a 2D calculation.

### 2.2.2 Proper Generalized Decomposition

The main problem associated with the increase of the wave scattering problem dimensionality is that it causes an exponential increase in the computational capacity required to obtain a solution. When Proper Generalized Decomposition is introduced, the complexity of the problem scales linearly instead. Circumventing the bottleneck that a fully scaled 4D wave propagation model would suppose to the mainstream processing power existing nowadays.

This section describes the general principles of the PGD and illustrates the basic methodology to obtain the successively enriched solution by means of a greedy algorithm strategy. The high-dimensional solver used to obtain  $u(x, y, \omega, \theta)$  is based in the offline construction of the  $n$ -rank separated form of free surface elevation, namely:

$$u(x, y, \omega, \theta) \approx u^n(x, y, \omega, \theta) = \sum_{m=1}^n F_1^m(x, y) F_2^m(\omega) F_3^m(\theta) \quad (2.11)$$

The PGD algorithm aims to determine the necessary  $n$  terms to obtain the functions  $F_1^m$ ,  $F_2^m$  and  $F_3^m$  for  $m = 1, \dots, n$ . Once the functions in (2.11) are known, it is possible to quickly determine any value of  $u^n$  by a fast linear combination.

The determination of each  $m$  term is carried out by means of the greedy algorithm, adding an additional rank-one element in each step:

$$u^n(x, y, \omega, \theta) = u^{n-1}(x, y, \omega, \theta) + F_1(x, y) F_2(\omega) F_3(\theta), \quad (2.12)$$

Where:

$u^{n-1}$  is the known value of the previous term.

$F_1$ ,  $F_2$  and  $F_3$  are the separated functions of the  $n$  unknown term.

Introducing the (2.12) progressive solution in the (2.9a) weak form of the problem statement yields the following non-linear expression to be solved:

$$A(F_1 F_2 F_3, \delta u) = L(\delta u) - A(u^{n-1}, \delta u) \quad (2.13)$$

Various approaches exist to solve the weak form of the PGD in (2.13). Previous studies by Modesto (2014) have shown that, due to the non-hermitian nature of the MSE problem, the Petrov-Galerkin PGD approach is the most robust algorithm, even achieving solutions on occasions where the Standard approach would fail. Thus, a general description of the Petrov-Galerkin PGD approach is given next.

The test functions  $\delta u$  are considered as a combination of separated functions denoted as:

$$\delta u = \delta F_1 F_2 F_3 + F_1 \delta F_2 F_3 + F_1 F_2 \delta F_3. \quad (2.14)$$

The Petrov-Galerkin PGD can be interpreted as an *a priori* model reduction technique, in which a fixed-point algorithm is used to determine the functions  $F_1$ ,  $F_2$  and  $F_3$  with the use of auxiliary functions. In this algorithm, the test functions  $\delta u$  from the Eq. (2.13) are substituted by  $\delta \tilde{u}$ :

$$A(F_1 F_2 F_3, \delta \tilde{u}) = L(\delta \tilde{u}) - A(u^{n-1}, \delta \tilde{u}) \quad (2.15)$$

Where:

$$\delta \tilde{u} = \delta \tilde{F}_1 \tilde{F}_2 \tilde{F}_3 + \tilde{F}_1 \delta \tilde{F}_2 \tilde{F}_3 + \tilde{F}_1 \tilde{F}_2 \delta \tilde{F}_3$$

In order to obtain the  $\tilde{F}_1(x, y)$ ,  $\tilde{F}_2(\omega)$  and  $\tilde{F}_3(\theta)$  auxiliary functions, the following problem must be solved for all  $\delta u$  in the form of Eq. (2.14):

$$A(\delta u, \tilde{F}_1 \tilde{F}_2 \tilde{F}_3) = (\delta u, F_1 F_2 F_3)_{\Omega \times I_\omega \times I_\theta} \quad (2.16)$$

The substitution of the  $\delta u$  in (2.15) and the auxiliary functions  $\tilde{F}_1(x, y)$ ,  $\tilde{F}_2(\omega)$  and  $\tilde{F}_3(\theta)$  in (2.16) form a non-linear system for the function pairs  $(F_1, \tilde{F}_1)$ ,  $(F_2, \tilde{F}_2)$  and  $(F_3, \tilde{F}_3)$  that can be solved using a fixed-pointed algorithm consisting of three stages. In each of the stages, two of the function pairs outlined above are assumed to be known, and the third one is determined through the non-linear system made up by (2.15) and (2.16):

1. Assume that the  $(F_2, \delta \tilde{F}_2)$  and  $(F_3, \delta \tilde{F}_3)$  pairs are known, and compute the two linear bidimensional problems to determine  $(F_1, \tilde{F}_1) \in \mathcal{H}^1(\Omega)$ , for all  $(\delta F_1, \delta \tilde{F}_1) \in \mathcal{H}^1(\Omega)$  satisfying:

$$\begin{aligned} A(F_1 F_2 F_3, \delta \tilde{F}_1 \tilde{F}_2 \tilde{F}_3) &= L(\delta \tilde{F}_1 \tilde{F}_2 \tilde{F}_3) - A(u^{n-1}, \delta \tilde{F}_1 \tilde{F}_2 \tilde{F}_3) \\ A(\delta F_1 F_2 F_3, \tilde{F}_1 \tilde{F}_2 \tilde{F}_3) &= (\delta F_1, F_1)_\Omega (F_2, F_2)_{I_\omega} (F_3, F_3)_{I_\theta} \end{aligned} \quad (2.17a)$$

After solving (2.17a) the pair of functions  $(F_1, \tilde{F}_1)$  are  $\mathcal{L}^2$  normalized.

2. Assume now that the  $(F_1, \tilde{F}_1)$  and  $(F_3, \tilde{F}_3)$  pairs, from the previous step, are known. Solve two linear 1D problems to evaluate  $(F_2, \tilde{F}_2) \in \mathcal{L}^2(I_\omega)$ , for all  $(\delta F_2, \delta \tilde{F}_2) \in \mathcal{L}^2(I_\omega)$  satisfying:

$$\begin{aligned} A(F_1 F_2 F_3, \tilde{F}_1 \delta \tilde{F}_2 \tilde{F}_3) &= L(\tilde{F}_1 \delta \tilde{F}_2 \tilde{F}_3) - A(u^{n-1}, \tilde{F}_1 \delta \tilde{F}_2 \tilde{F}_3) \\ A(F_1 \delta F_2 F_3, \tilde{F}_1 \tilde{F}_2 \tilde{F}_3) &= (F_1, F_1)_\Omega (\delta F_2, F_2)_{I_\omega} (F_3, F_3)_{I_\theta} \end{aligned} \quad (2.17b)$$

After solving (2.17b) the pair of functions  $(F_2, \tilde{F}_2)$  are  $\mathcal{L}^2$  normalized.

3. Assume now that the  $(F_1, \tilde{F}_1)$  and  $(F_2, \tilde{F}_2)$  pairs are known from the two previous steps. The separated functions in the incoming direction domain,  $(F_3, \tilde{F}_3) \in \mathcal{L}^2(I_\theta)$ , are found for all  $(\delta F_3, \delta \tilde{F}_3) \in \mathcal{H}^1(\omega)$  as the solution of:

$$\begin{aligned} A(F_1 F_2 F_3, \tilde{F}_1 \tilde{F}_2 \delta \tilde{F}_3) &= L(\tilde{F}_1 \tilde{F}_2 \delta \tilde{F}_3) - A(u^{n-1}, \tilde{F}_1 \tilde{F}_2 \delta \tilde{F}_3) \\ A(F_1 F_2 \delta F_3, \tilde{F}_1 \tilde{F}_2 \tilde{F}_3) &= (F_1, F_1)_\Omega (F_2, F_2)_{I_\omega} (\delta F_3, F_3)_{I_\theta} \end{aligned} \quad (2.17c)$$

Even if two systems of equations need to be solved at the end of each stage in (2.17), the solutions for  $\tilde{F}_i$  and  $F_i$  where  $i = 1, 2, 3$  generate the same matrix, so the computational cost is not duplicated.



## Chapter 3

# The real-time application tool

This Chapter presents and discusses several applications of interest for the practices of coastal engineering and harbour management that can be obtained with the methodology described in Chapter 2. The resulting outputs are implemented in a Graphical User Interface developed as a demo of the functionalities and capabilities of the software. The source of many of the outputs is a mix of research, thought and information given by several professionals related to the field of application. It is not meant to englobe all the possible inputs and outputs of the harbour agitation problem, as the criteria for their selection and implementation has been conditioned by their perceived usefulness and adequacy to the model adopted in this thesis.

The first section gives an overview of the most widely-used outputs in coastal engineering and design, with a discussion on their adequacy and possible adaptation to the wave monitoring tool. Several selected outputs and inputs are presented, with the method used to obtain them and their application to the coastal engineering field.

The other section discusses the challenges and the methodology used to implement these applications on an integrated software capable of evaluating these queries in real-time.

### 3.1 Outputs of interest for harbour models aimed towards coastal engineering

While most studies in the field of coastal engineering mainly focus on the wave height as the output with greatest interest for the practices of harbour engineering and design, there is an extensive number of variables or data visualization modes that can be obtained in conjunction or derived from the wave height.

The list of possible solutions offers a wide range of applications of interest to the optimization of coastal engineering, design and maintenance. What follows is a list of several key variables that can be easily evaluated as a function of the  $u(x, y, \omega, \theta)$  particularized

solution.

### 3.1.1 Real-time solutions for any particularized mesh node

One of the most critical outputs for any large spatial domain is to find singular values on the spatial dimensions. This is specially interesting when a high physical accuracy is required. Examples of this application include small vessel manoeuvres and operations, localized resonant responses or sediment accumulation zones.

The solution is a singular point in the spatial  $(x, y)$  and parametric  $(\omega$  and  $\theta)$  dimensions. Thus, the solution is unique in all dimensions:

$$u_{i,j,k} = u^{\text{PGD}}(x_i, y_i, \omega_j, \theta_k) \quad (3.1)$$

Where  $i, j$  and  $k$  are the indexes of the closest mesh node to the user-selected element spatial, frequential and directional coordinates, respectively.

When the user selects a spatial point for the current directional and frequential snapshots, the localized solution is displayed on a textbox with the coordinates of the closest node to allow a higher degree of precision with the observation of the results.

A vast part of wave resonance studies use this feature to present the results by showing the wave height distribution on a single point for a given set of input parameters, albeit with a much smaller degree of interaction, see Losada et al. (2008); Lee et al. (1998). Due to its accuracy, this output is also often used to compare numerical results to real-life historical data, which is only tracked on control points in most harbours.

### 3.1.2 Wave Height

Defined as the difference of a crest with its neighbouring trough, wave height is the main magnitude studied in the harbour wave propagation problem. This makes it the most relevant parameter to evaluate the validity of the obtained results, and consequently an accurate indicator of the model's reliability. It defines the sea state, and in linear models it is an accurate indicator of the wave energy.

In this thesis, the wave height is the only output that is directly stored in the full generalized solution. The computation for any single value pair of input parameters is carried out through the evaluation of the four dimensional  $H(x, y, \omega, \theta)$  solution matrix in the  $H(\omega, \theta)$  parametrized dimensions to obtain the bidimensional  $H(x, y)$  scalar field at a negligible cost. This field is then interpolated between the nodes that compose the mesh following a 4th order element scheme, obtaining accurate results even when dealing with irregular geometries:

$$H_{ij} = H^{\text{PGD}}(x, y, \omega_i, \theta_j) \quad (3.2)$$

The interface developed in this thesis plots the obtained colormap in a 3D environment, aiming to increase the realism of the visualization of the results. The obtained surface is also scaled to help a comfortable visualization of the data, and the option to adjust the transparency is provided to the user. This means that if the user were to opt to visualize the data with additional layers, which will be presented in the GUI section (3.2.3) later, such as bathymetry surface or the port's orthophoto, they would be able to see them simultaneously, allowing, for instance, the analysis of the effect of the bathymetry on the final solution.

Additionally, the high versatility of the PGD combinations allows to achieve the solution with a broad set of both individual and combined queries. The first ones represent a realistic situation, in which any given incoming wave is characterized by a single combination of period and direction, while the later ones allow the user to analyse the effects of several queries simultaneously and obtain combinations of interest for the engineering practice.

### 3.1.3 Limit Height

Safety assessments in harbour operations often have designated a threshold in wave height which, if surpassed, would indicate a serious risk for the naval operations in place or even the integrity of the vessels and harbour infrastructure. Many studies have used such measures as benchmarks with which to assess the overall safety and operability of a port. If these assessments are negative, the economic loss on a large logistic hub could be significant, as shown by Wood and Good (2004), increasing the need for a quick and effective way to establish a threshold on wave height.

One of the functionalities of the demonstrator allows to quickly establish a limit to the values of any evaluated parameter, so that only the waves that reach higher altitudes are highlighted.

### 3.1.4 Spectral distributions

Spectral distribution functions enable the statistical evaluation of long-term sea-state behaviour. Measuring the wave height against the wave period or incoming direction is an essential part of the spectral study of the wave parameters. Retroactively, using previously generated spectra as inputs on a wave combination function would allow to instantly perform a statistical evaluation of the long-term behaviour of the wave propagation problem.

Composed either by a combination of the full or partial range of input queries available in the generalized solution, this output allows to combine the individual solutions in a

single scalar field through the use of a spectral distribution that determines the probability densities of each individual solution:

$$U^C = \sum_{ij} w_{ij} u(x, y, \omega_i, \theta_j) \quad (3.3)$$

Where  $w_{ij}$  is the weight associated to the  $u(x, y, \omega_i, \theta_j)$  solution corresponding to the  $\omega_i$  and  $\theta_j$  queries.

As mentioned in the previous section, the combined solutions of several different incoming waves may prove useful in long-term evaluations of safety and operability. They can also be used for the parametrization of the physical domain, by analysing the combined response of the weighted incoming waves and their similarity to the real data on harbour agitation under the same conditions. The combination of several solutions can provide design waves that can be used for the optimization of future breakwater design or the increase of the efficiency of dredging operations.

Nevertheless, the most promising aspect of the combined solutions is the possibility for the user to define any possible combination function that takes the wave height parameter as input. Mean, significant wave heights, weight functions corresponding to the histograms of any period in time, future wave prediction data, are only some of the feasible outputs that can be instantly obtained from the PGD domain once the user uploads the desired function.

Combined solutions can also be used to describe any other physical magnitude related to the wave height field. This means that any user who may wish to add another scalar output that can be represented in the existing mesh can do so by adding an algorithm to obtain it from the wave height field, effectively allowing for any other feasible output to be added to the program in the future without needing to create another set of functions for it. Combinations of other physical variables can also be used for other purposes. For instance, using a weighted function with the histogram of incoming wave directions and periods to combine a wave potential solution would give a general idea of where the highest energy concentrations may be located in the future, helping in the location of the optimal implementation points for a wave farm.

Next, a slight differentiation is made between the combinations that use the full PGD range and those who only use a partial range.

### Full range solution

The full range solution combines all the existing scalar vectors from the generalized solution into a combined field in the physical domain by means of a user-specified function. The function specified by the user can have several different forms, such as average solution, weighted average of all solutions, minimum or maximum:

$$U^C = f(u^{\text{PGD}}) \quad (3.4)$$

Where  $f(u^{\text{PGD}})$  is the user-specified function.

### Partial range solution

There is also the possibility to implement user functions in a user-limited query range, instead of adopting the full range of input parameters offered by the generalized solution, a functionality that would result of interest in several situations. For instance, it would allow to combine just the frequencies and directions of the incoming waves generated by just one adverse sea state, which would exhibit a much more limited range of input parameters.

This feature can be used by assigning a null weight to the elements that are out of the desired range, and create a user function that evaluates the solutions that fall inside the given range:

$$U_{\partial}^C = \sum_{i_{\min}}^{i_{\max}} \sum_{j_{\min}}^{j_{\max}} f(u^{\text{PGD}}) \quad (3.5)$$

Where  $i_{\min}$ ,  $i_{\max}$ ,  $j_{\min}$  and  $j_{\max}$  are the indexes of the minimum and maximum frequency and direction, respectively.

### 3.1.5 Protective Index

The protective index of a wave field is an inverse measurement of the spatial distribution of the wave height. It is a convenient way of assessing which areas are better suited for port operability and safety, and it can also be used to find inefficiencies in harbour design, as shown in the study by Chakrabarti (1999).

Its computational cost is almost non-existent, as merely the inverse of the wave height has to be evaluated for all spatial points:

$$IP_{ij} = H_{ij}^{-1} \quad (3.6)$$

### 3.1.6 Wave Potential

The energy that can be obtained from wave currents is enormous. The amount of current electricity consumption in the world pales in comparison with the amount of wave energy that can be extracted, and this in turn is orders of magnitude below what is available in the ocean. It is estimated that European waters can provide more than 50% of the continent's energy needs. Several studies in recent years have shifted their focus towards

this reachable source of energy, but few are still the sites in which it has become a reality. Studies such as the one by Iglesias et al. (2009) have shown that one of the best areas to install wave farms is on the depths close to the harbour, as the energy and resources to make use of the energy are far smaller than a full off-shore platform. Low efficiency models existing nowadays also help decrease the gap between the offshore and nearshore farms, with nearshore farms being far more efficient in energy extraction. An initial estimation of the sea's energy output can be the perfect indicator when deciding the layout of the breakwater structures and energy capturing devices.

This thesis includes the Wave Potential output as the amount of energy per meter length that could be extracted at any point. The potential energy that is contained per wave width meter is directly related to the wave height by means of the following expression:

$$P = \frac{g^2 \rho H^2 T}{32\pi} [\text{kW/m}] \quad (3.7)$$

This means that wave potential increases proportionally to the square of the amplitude of the wave, making the energetic output for the long-period waves (7-10 s) and high amplitudes (in the order of 2 metres) exceed in many cases the 40 – 50 kW/m values. The physical explanation for this behaviour relies on the fact that the elliptic movements adopted by water particles in any given point on the wave increase with height, so the particles on the surface of a wave carry a greater amount of energy as the wave propagates. Energy capturing devices also have the added advantage of the dissipation of other forms of energy that may not result beneficial to the nearby structures.

Additionally, by combining this variable to the spectral solutions outlined in 3.3, it would be possible to assess the theoretical energetic yearly output for any harbour, making it easier to determine the feasibility and investment return of energetic exploitation projects on the site.

### **3.1.7 Resonance studies**

Wave resonance studies are among the most widely used applications of the harbour wave agitation problem. Comparing the wave heights in a single spatial point through all frequencies and directions allows to quickly assess which periods and directions can prove to be a hazard for the naval operations or the safety of all parties involved. Several examples of these studies can be found by Guerrini et al. (2014); Bellotti (2007); Losada et al. (2008); Vela et al. (2014); Lee et al. (1998).

In addition to the variable fields generated from plotting the generalized solution in the frequential and directional dimensions to get a spatial distribution of the desired magnitude, it is also possible to employ the same procedure in the spatial dimensions

to get the desired parametric distribution. This distribution can be used to identify the dependence of the solution to the different input parameters' values. The method of data visualization can be either in bidimensional or tridimensional form, depending on the amount of dimensions the results are to be showed in.

### Direction range distribution

One of the parameters whose effects can be modelled is the incoming wave direction. In this case, the PGD function work on the spatial and frequential dimensions, displaying the wave height distribution along all directions for the current frequency and only for the user-selected spatial point. The resulting vector is plotted in a 2D graph:

$$u_{ij} = u^{\text{PGD}}(x_i, y_i, \omega_j, \theta) \quad (3.8)$$

This enables the possibility to observe and study the effects of the incoming wave direction on any of the aforementioned magnitudes, and thus identify which incoming wave directions are desirable, for wave energy output, for instance, or to be avoided when planning logistic operations in the selected zone. If long periods are included in the generalized solution, this output can also highlight the critical directions under which a resonant response is given for each point in space.

### Period range distribution

The other possibility that the parametrized distribution approach provides is to observe the effect of the different periods in the localized solution. The method, in this case, evaluates the solution vector corresponding to the selected direction and spatial point, and plots it against all incoming wave periods to observe their effects on the solution:

$$u_{ij} = u^{\text{PGD}}(x_i, y_i, \omega, \theta_j) \quad (3.9)$$

The great usefulness of this output lies in its adequacy for wave resonance studies. If long periods were considered in the generalized solution, it would enable the user to instantly evaluate the resonance phenomenon in any spatial point with minimum computational cost.

### Directional and periodical distribution

The third parametric distribution combines the two outputs mentioned previously in a single 3D surface plot that can be instantly obtained for any given spatial point. This allows the user to observe the full distribution of the wave height at any point without

having to perform every single enquiry for all input parameters. The real-time solver generates in this case a matrix composed of the solution vectors for each input parameter instance, making its calculation slightly more expensive than the 2D distributions:

$$u_i = u^{\text{PGD}}(x_i, y_i, \omega, \theta) \quad (3.10)$$

While the generated surface is not as easy to study as the previous outputs, the possibility to mark, for each spatial point, the worst combination of incoming wave frequency and direction allows to easily identify the critical incoming parameter pair, as opposed to the single critical frequency or direction that may not find the global maximum on the surface generated for the selected point.

### **3.1.8 Spatial solution**

In addition to the full spatial solutions obtained by obtaining the generalized solution for the given set of queries, the physical variable field can be further reduced to a localized area or single point. If this possibility is combined with the expanded parametrized distribution outputs mentioned earlier, a full 4D analysis can be performed on the solution matrix without the need to perform each calculation individually. Combining the reduced spatial truncation that an user-specified selection provides with the reduced-range combination of the solution that was mentioned on the Spectral distributions (3.1.4) section allows to further truncate the solution matrix in any or all of the 4 dimensions that compose the generalized solution.

#### **Single-point solution**

Several studies in which the Wave Height (3.2) was observed also focused on the minimum and maximum values of the wave field to benchmark the port's effectiveness in reducing wave amplitudes. Obtaining the minimum and maximum variable values is also possible using a simple function triggered by the localized area solution explained next.

#### **Reduced area solution**

Finally, many applications in harbours require the study of a reduced area of interest for many different applications, see the study by Diaz-Hernandez et al. (2015) for instance. For that, the reduced area selection allows to evaluate the distributions in (3.9), (3.8) and (3.10) with in conjunction with the maximum and minimum queries presented in (3.1.8). It also has the additional functionality to select a “representative wave” in the selected region, which can be a minimum, maximum or average wave height of the reduced area. The aforementioned distribution functions plot the effects of the incoming wave period and

direction on the point that is selected according to the previous user selection (maximum, minimum or average), allowing, for example, to evaluate the worst-case scenario of the point with maximum current wave surface elevation.

## 3.2 Implementation and GUI design

The main objective of this thesis is to provide an integrated environment in which all these queries are evaluated in real time with a high degree of user interaction. A Graphical User Interface is the most widely used method whereby information systems interact with users. The applications for the tool are many, from being able to predict the immediate incoming wave climate from the port buoy itself to obtaining long term design waves with which to test a proposed new geometric layout or a new dredging operation. Creating a tool with such a high versatility has many challenges, both numerical and functional. What follows is a general description of the inner workings of the interface, with descriptions of the file system in (3.2.1), the data structure in (3.2.2) and finally a general description of the layout and the elements in the GUI in (3.2.3).

### 3.2.1 Description of the file system

The software has been developed in a MATLAB<sup>©</sup> environment, structured as a combination of a main UI file which uses data and callbacks located in the program folder. The structure of the file system is distributed as follows:

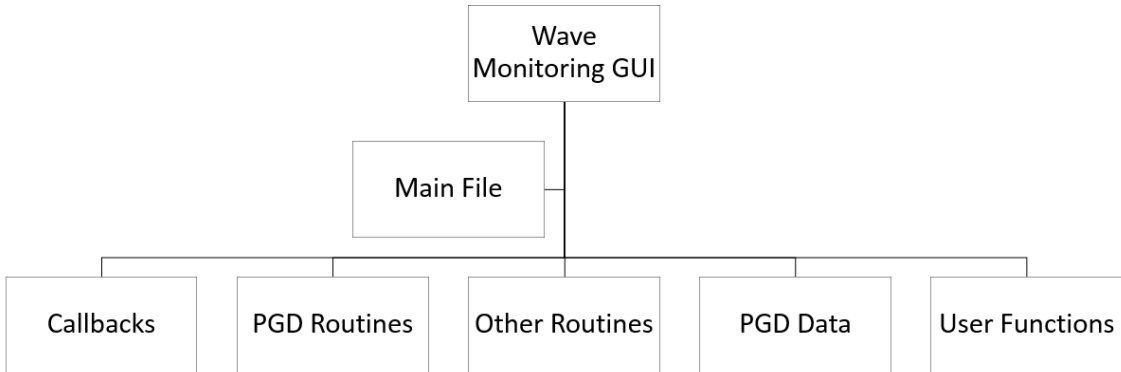


Figure 3.1: GUI folder structure

The main file has the function of creating the main GUI layout, the variable structure to be used by all the functions, and assigning the specific callbacks for each UI element and function. When it is executed, these tasks are carried out following this sequence:

1. Generation of figure, still invisible.
2. Creation of the axes in which the plots will later be drawn.

3. Definition of the rest of user interface elements such as tools, UI Panels, and UI Controls.

- (a) Tools are singular callback buttons that link to a specific function. They are toggled when the user clicks on them, enabling functionalities that are otherwise disabled.



Figure 3.2: GUI tools

- (b) UI Panels are containers in which other elements are grouped together.
- (c) UI Controls are user interface control objects. When selected, they perform a specific action determined by the callbacks they are linked to. They can adopt many different styles, i.e. check-box, list-box, radio button, push button, slider, text, toggle button, to name a few, according to their suitability for the function they are linked to.

4. Assign tags to each element.

5. Definition of the data and handle structures.

6. Set user interaction functions.

7. Assign callbacks to each interface element.

8. Initialization tasks, make figure visible.

The main GUI file calls upon functions and data located in the sub-folders.

The “Callbacks” sub-folder contains functions that are linked to certain UI elements or gestures, and triggered after a certain action has been performed by the user (execute the main file, load a port, click on a single spatial point in the plot, select a region from the plot surface, change the input parameters or move a slider, for instance). They are the source of all the interactive possibilities that the GUI displays, and in many occasions data is shared between several of them. Special care has to be taken with the callbacks that share variables, as conflicting uses of the same data such as deletion or modification of properties can render it useless to other functions, which may cause the software to stop working altogether. A way to avoid creating redundant data while preventing conflicts between callbacks is to define which function should be executed by a very specific set of conditional operators. An example of the decision tree for the function associated with the “mouse button motion” action is given next. This function is triggered whenever the pointer is moved in the figure, and it can perform a different set of actions depending on

the previous callbacks that were executed and the presence of certain variables. What follows is a simplified scheme in which the conditions and consequences of each possibility are outlined:

```

function ButtonMotionFunction

if Button Functions are enabled (an example has been loaded)
    Determine current axes.
    if Current axes = Arrow axes
        if The mouse button is pressed
            if A region was previously selected
                Delete region selection.
            end
            Update arrow drawing and incident wave parameter
            values.
        if Spectral distribution graphs exist
            Update current value of parameters in
            graphs.
        end
        if A single spatial point was previously
        selected
            Delete spatial point information.
        end
    end
    elseif Current axes = Main Plot axes
        if Current coordinate indicators are enabled
            Update coordinate indicators.
            if A region selection was started (The user is
            dragging the pointer in the main plot)
                if A single point selection exists
                    Delete single point selection
                    textbox.
                end
                if Current tab = Tab 1
                    Set axes 1 as parent object.
                elseif Current tab = Tab 2
                    Set axes 2 as parent object.
                elseif Current tab = Tab 3
                    Set axes 3 as parent object.
                elseif Current tab = Tab 4
                    Set axes 4 as parent object.
                end
                if This is the first region selection
                    Draw rectangle for the first
                    time.
                else (If there is another rectangle
                    present)

```

```

    Change current rectangle
    coordinates.

    end
end
end
end

```

The above function is called upon whenever the pointer is moved, so special care has to be taken with the treatment of shared variables so as to avoid conflict with other callbacks that rely on them. This is specially true for functions that can perform a variety of actions depending on the previous callbacks that were executed, so taking into account all possibilities becomes a crucial condition for the reliability of the program and bug prevention.

As a consequence of this condition, the amount of precautions needed to be taken grows exponentially with the complexity of the program and the number of functions. Callbacks that are triggered by the same action (i.e. a mouse double-click) can have completely different functions associated to them depending on the conditions in which the triggering action was performed.

Many of these callbacks rely on the functions that are stored on the “PGD Routines” and “Other Routines” folders. The former ones are aimed towards the handling of the PGD data, while the files stored in the later are auxiliary functions necessary to execute several tasks on the interface.

The variables that these functions access are extracted from the “PGD Data” folder during the PGD loading callback sequence. A tool with such a high degree of complexity as this one requires a well-defined variable structure in order to effectively share data between functions without conflicts arising. More on that aspect will be explained in the Data structure subsection (3.2.2).

The User Functions folder, on the other hand, holds the user-generated spectrum functions. This folder is accessed at startup, and the initialization routine loads all the functions present there to make them available to the user via the relevant interactive drop-down menu. The files contained in this folder are accessed each time a new combination is selected from the GUI to generate a new user-determined wave. In other words, it is a folder in which user-generated functions are stored to be later executed by a single callback.

### **3.2.2 Data and handles structures**

In the previous part (3.2.1), the importance of storing all variables on a single well-organized structure was highlighted. With such an ample range of functionalities as the ones present in this development, the variables to be stored require a great variety of

formats. Coefficients, solution matrices, vectors, boundary parameter values, and other existing variables are allocated into the following structure by the associated callback function once the PGD data is loaded:

```

dir_struct = Directory structure to locate PGD files.
plotid = Solution plot handles.
arrowid = Incident wave input arrow handle.
bottomid = Handle to bottom surface plot.
arrowdata = Incident wave input arrow data.
backgroundid = Handle to background orthophoto.
userSelection = Logical operator to determine the next callback function
    , depending on the previous behaviour of the user. If a buttondown
    action has been performed previously, userSelection = true.
Pointer = Data containing current pointer position.
CurrentTab = Variable of currently selected tab.
PortNames = Cell string that shows the names of the ports found in the
    PGD Data folder.
PortCoordinates = Vectors that show the coordinates of the ports found
    in the PGD Data folder.
colorbarid = Handle to solution plot colorbars.
PortMarkers = Handle to interactive port loading markers.
ButtonFunctionsFlag = Logical operator to determine if interactive
    functions are enabled or disabled.
SelectionPoint = Location of the cursor when a buttondown action was
    performed.
bottom = Bathymetry surface variables for each mesh node.
meshid = Handle to mesh plots.
boundaryid = Handle to boundary plots.
graphid = Handle to 2D parametric distribution plots.
lineid = Handle to current parameter value lines in 2D parametric
    distribution plots.
solution = Full PGD solution combination.
rectSelection = Coordinates of the user-selected reduced area.
rectSelectionid = Plot handle to the user-selected reduced area.
rectInipoint = Initial point of rectangle, necessary for rectangle
    functionality.
surfid = Handle to the 3D parametric distribution surface.
rectid = Handle to the rectangles used to show current parametric values
    in 3D distribution plot.
limitid = Handle to the rectangle surface used to highlight the solution
    above the user-specified limit.
locationPlot = Handle to the map in which the port location markers are
    shown.
PlotMarkerCoordinates = Vectors with the coordinates of the loaded port
    markers in the locationPlot axes.
background = Image data from which backgroundid is created.
pgd = PGD data.
```

```

PGDalgorithm = Data on the PGD algorithm that was used to achieve the
    PGD solution.

parameters = A set of useful parameters for the characterization of the
    PGD solution.

PGDmeshes = PGD solution mesh structure. Gives information on spatial
    and parametric dimensions.

OPTmeshes = Secondary PGD solution mesh structure. Gives information on
    the parametric dimensions.

snapshot = A pair of values representing the current wave frequency and
    direction.

nOfPGDterms = Value showing number of PGD terms used to accomplish
    current solution.

PlotAxesCoordinates = Value pair showing current pointer position on the
    plot axes coordinates.

```

Additionally, the sequence outlined in (3.2.1) creates a second structure containing handles. These are data types that store associations with functions or objects. In this thesis, each UI element is represented by its handle in the following structure:

```

MainFigure: [1x1 Figure]
Output_Panel: [1x1 Panel]
Plot3D_Text: [1x1 UIControl]
Theta_Text: [1x1 UIControl]
Omega_Text: [1x1 UIControl]
UserFcn: [1x1 UIControl]
UserFcn_Text: [1x1 UIControl]
Info_Panel: [1x1 ButtonGroup]
Coord_Panel: [1x1 Panel]
Input_Panel: [1x1 Panel]
View_Panel: [1x1 Panel]
PGD_Panel: [1x1 Panel]
MainTabs: [1x1 TabGroup]
axes3D: [1x1 Axes]
axesTheta2D: [1x1 Axes]
axesOmega2D: [1x1 Axes]
axesArrow: [1x1 Axes]
axesLocation: [1x1 Axes]
Text_Output: [1x1 UIControl]
Maximum_Value: [1x1 UIControl]
Maximum_Text: [1x1 UIControl]
Minimum_Value: [1x1 UIControl]
Minimum_Text: [1x1 UIControl]
Average_Value: [1x1 UIControl]
Average_Text: [1x1 UIControl]
YCoord_Value: [1x1 UIControl]
YCoord_Text: [1x1 UIControl]
XCoord_Value: [1x1 UIControl]
XCoord_Text: [1x1 UIControl]

```

```

PGDTerms_Value: [1x1 UIControl]
PGDTerms_Text: [1x1 UIControl]
Direction_Value: [1x1 UIControl]
Direction_Text: [1x1 UIControl]
Period_Value: [1x1 UIControl]
Period_Text: [1x1 UIControl]
Freq_Value: [1x1 UIControl]
Freq_Text: [1x1 UIControl]
View_BotTransparency: [1x1 UIControl]
View_BGTransparency: [1x1 UIControl]
View_MeshTransparency: [1x1 UIControl]
View_PlotTransparency: [1x1 UIControl]
View_BC: [1x1 UIControl]
View_Background: [1x1 UIControl]
View_Plot: [1x1 UIControl]
View_Bottom: [1x1 UIControl]
View_Mesh: [1x1 UIControl]
View_Axes: [1x1 UIControl]
DirectionRange_Value: [1x1 UIControl]
DirectionRange_Text: [1x1 UIControl]
PeriodRange_Value: [1x1 UIControl]
PeriodRange_Text: [1x1 UIControl]
ElemType_Value: [1x1 UIControl]
ElemType_Text: [1x1 UIControl]
Rotate: [1x1 ToggleTool]
PanXY: [1x1 ToggleTool]
ZoomXY: [1x1 ToggleTool]
Tab1: [1x1 Tab]
Tab2: [1x1 Tab]
Tab3: [1x1 Tab]
Tab4: [1x1 Tab]
axesPlot1: [1x1 Axes]
axesPlot2: [1x1 Axes]
axesPlot3: [1x1 Axes]
axesPlot4: [1x1 Axes]

```

This structure is created at the GUI startup sequence, and it assigns a handle to every UI element through its tag property. The purpose of these handles is to access and modify the properties and information stored in the components they link to. For instance, going back to the “Button Motion Function” example earlier, the determination of the currently active tab is carried out by identifying the value of its “Selected” property.

Overall, the purpose of the data and handle structures is to simplify the organization of all the relevant variables and handles present in a complex environment containing a large number of functions and files, providing a clear understanding of the behaviour of conflicting functions on common elements and data.

### 3.2.3 Layout and elements description

This section discusses the layout used to present all the functionalities to the end user. Providing a clear platform to facilitate a clear understanding of the results and allowing the maximum degree of interaction for the user is crucial for the appeal of the software developed in this thesis.

With that goal in mind, a single layout containing all the necessary elements is presented:

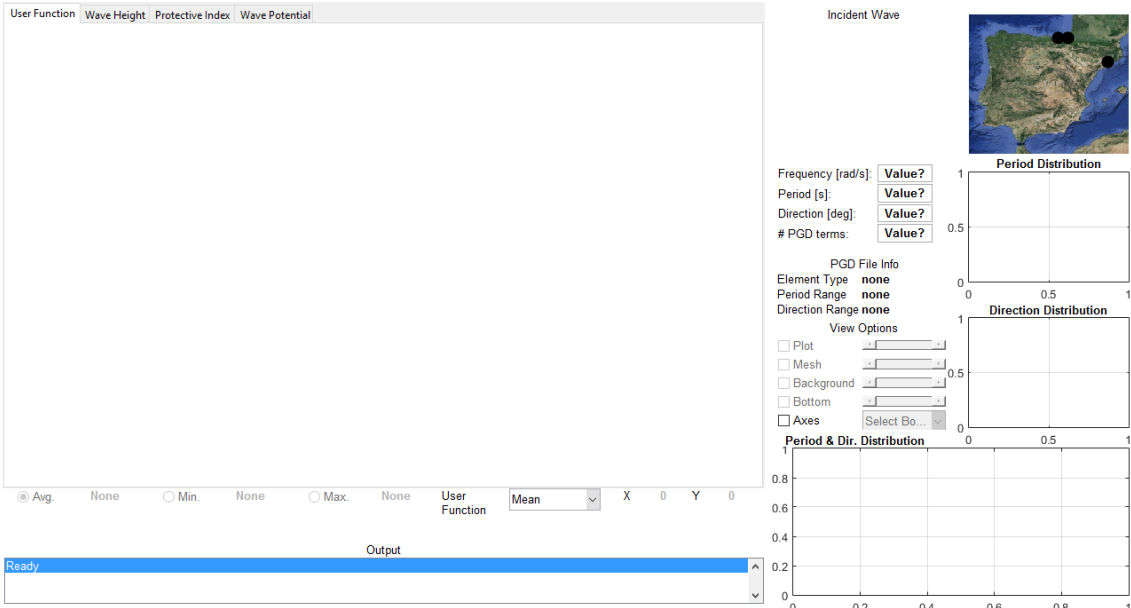


Figure 3.3: Graphical User Interface layout

As can be seen in figure (3.3), most of the functionalities of the tool are disabled until an example is loaded. The purpose of this measure is to guide the user towards the element from which data corresponding to a port can be loaded. This function can be triggered by double-clicking on a port marker in the port location map, located on the upper right side of the layout presented in (3.3):



Figure 3.4: Port Selection Map: The selected port's information is shown in the textbox prior to the loading sequence

When a port is loaded, the solution data that has to be converted into variables is extracted from the PGD Data folder. Here, each port has a sub-folder in which the generalized solutions, port location data, ortophoto and several other parameters of interest (contour nodes, absorption coefficients, finite element type...) are stored to be later loaded by the relevant functions. These folders are accessed on the initialization stage, and the interface loads all the ports that are present in them. When a single click is made on a por marker, the relevant information stored in its folder is displayed in the map by means of a textbox, as shown in (3.4).

When all the variables are identified, the PGD loading routine looks into the port data for several useful parameters that give information on the generalized solution. Parameters such as the range of modelled periods and directions give the engineer the necessary information to know which type of waves are being modelled, or allow a quick comparison with any existing histogram to determine the degree of coverage of the usual incoming wave conditions present in the area. These and other parameters are shown in the “PGD File Info” panel, located on the right of the main plot axes:

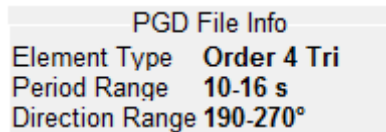


Figure 3.5: PGD information panel

Once the variables have been allocated into the GUI structure, the second stage of the loading phase is launched, which involves creating the initial plots for the selected example. These are allocated to the main plot axes contained in the following tabs, to allow the user to easily switch the visualized information while keeping all functionalities intact between different tabs:

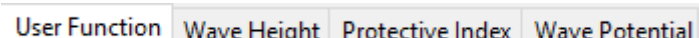


Figure 3.6: Scalar field selection tabs for the main plot axes

Another added advantage of the use of tabs is the reduction on the number of open windows when working with the program. Tabs allow a clear distinction on which scalar variable is active at every moment in the execution of the desired queries while sharing the functionalities provided by the other elements, creating a uniform environment devoid of discontinuities and hassle when transitioning from one variable to another.

An extra asset for data visualization is presented in the “View Panel”, located on the right of the main plot axes:

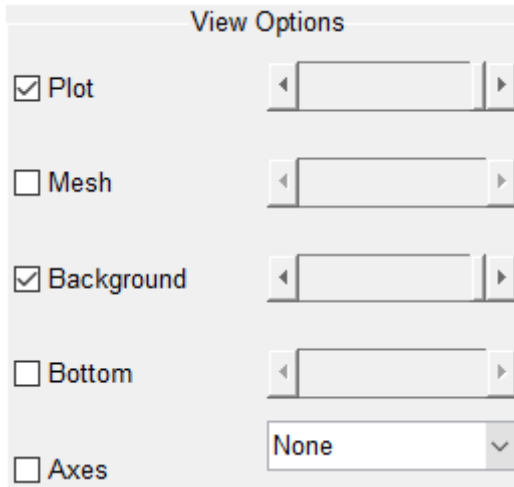


Figure 3.7: Scalar field data visualization options panel

The figure shown in (3.7) displays the available configurations for the visualization of the scalar data plotted in the tabs shown in figure (3.6). Four layers can be active at the same time: (i) A 3D surface of the scalar field in each tab; (ii) a plot of the mesh used to generate the solution, to allow clear location of nodes; (iii) a background image to aid in the localization and add realism to the results; and (iv) another 3D surface of the bathymetry of the modelled example. All except the first one are identical in every tab, as they describe static parameters that don't change with the input parameters. At any given tab, any combination of them can be active. To reduce the difficulties caused by overlapping different layers of data on a single set of axes, transparency sliders are provided for each layer, as can be seen on the immediate right-hand side of the main plot axes in the (3.7) figure. This allows several combinations of interest for an intuitive visualization of the desired data, allowing, for example, to observe the effects of the bathymetry on the current solution by adjusting the transparency setting on the top layer to a lower value. Finally, activating the “Axes” option allows to quickly view the coordinates around the plot and obtain the rough position of any given point visually. Nevertheless, with this purpose in mind, the alternative of using the coordinate panel, located on the lower right corner of the main plot axes in (3.3), is recommended over the axes feature, as it shows a greater precision by showing the coordinates of the pointer in the plot at any given time:

X 271.943 Y -186.739

Figure 3.8: Coordinate panel

Another feature of the “View Panel” can be seen on the lower-right corner of the figure in (3.7), in the drop-down menu whose current is value set to “none”. This drop down menu behaves in a similar way to the User Function drop-down menu explained in

(3.2.1), in the aspect that it loads all the boundaries present in the PGD data with their corresponding nodes on the solution loading sequence. These boundaries are then plotted at the request of the user, allowing to visualize the different contours that are present in the example.

Working on a similar manner to the “View Panel” is the feature that allows the user to specify a certain limit on the scalar field being observed. By selecting the desired height through the colorbar located on the right hand side of the main plot axes, the parts of the 3D surface plot that are below the selected point are shadowed, effectively allowing the user to set a threshold on the results that they want to observe.

Closely related to the view panel in its objectives of improving the visualization of the data as much as possible, is the tool palette. Previously shown in figure (3.2), these buttons are linked to callbacks specifically designed with the applications of this software in mind. Options for zooming, panning, and rotating in the 3D solution surface plots are given in a simple manner. Clicking any of the tools will toggle the associated mode on, disabling the other two in order to prevent conflicts.

The last visualization-oriented component is the “Output panel”. Located on the lower left side, this element gives information about the events and progress of the operations performed in the GUI. PGD data loading progress or interaction instructions are given in this panel, with the goal of guiding the user through the different possibilities that may not have been seen in the first viewing:

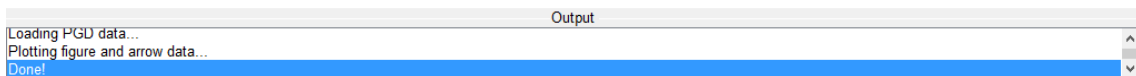


Figure 3.9: Output panel

## Interactive functionalities

The second objective outlined at the beginning of this chapter aims to provide the outputs discussed in (3.1) in real-time with the highest degree of user interaction. As it was mentioned in the “mouse button motion” example from (3.2.1), this functions are the most complex ones to implement, but also prove to be the ones that add most value to the applications of this thesis through their possibilities for interaction.

First, the “Incident Wave” panel is introduced. Located on the upper right corner of the layout seen in figure (3.3), this is a key element to provide the highest possible degree of user-friendliness to introduce incoming wave parameters:

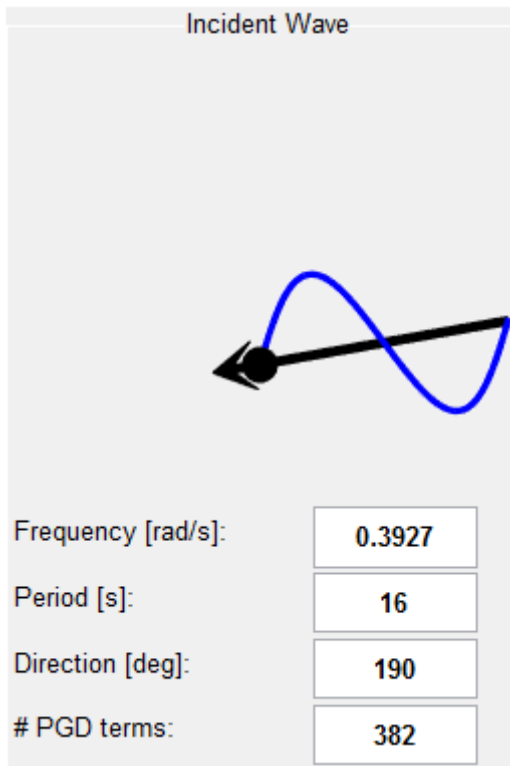


Figure 3.10: Incoming wave panel

In the panel shown in this image, the arrow on the top and the textboxes below share the same function: Specifying the incoming wave parameters. While the approach of the later ones is pretty straightforward, it adds the option to specify the number of PGD terms that the user wants to take into account when obtaining the solution. The arrow, on the other hand, is a completely different approach: It works by clicking and dragging the dot along the arrow length to change the incoming wave's period, while moving it around the imaginary centre of the component (located at the tip) causes a change in incoming wave direction. Both movements update the arrow to reflect the current position of the dot. This and the first option achieve a real-time solution for any desired queries included in the model, but the possibility to choose between them adds a remarkable degree of user-friendliness to the demonstrator.

In this thesis, an additional input method is implemented in the layout. It can be seen below the main plot axes in the (3.3) figure, shown as a drop down list:

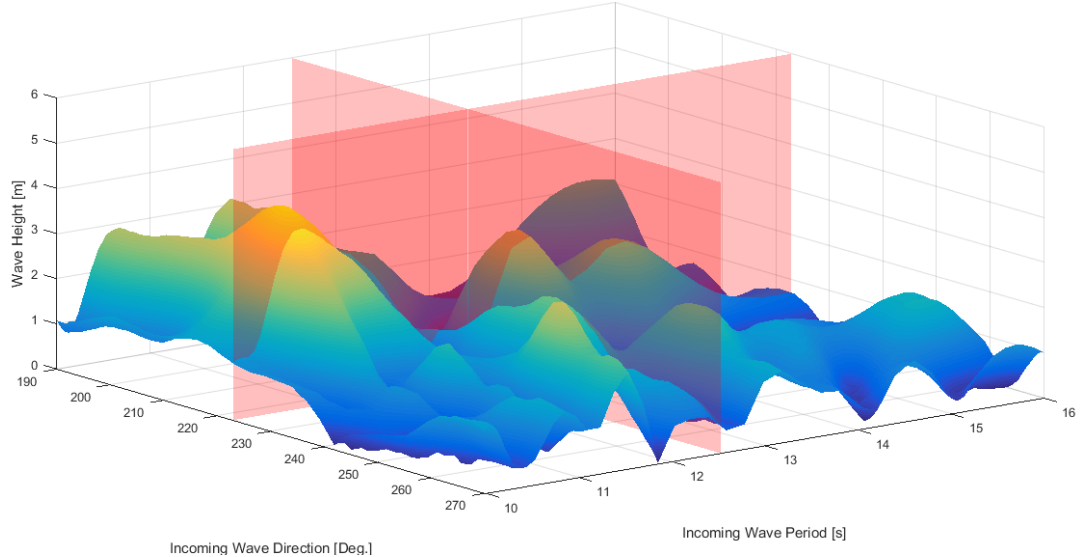


Figure 3.11: User function selector

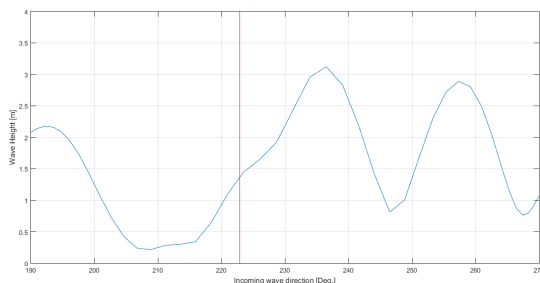
The great potential that the tool shown in this image holds relies on the fact that it allows the user to add any input functions with which the manipulation and combination

of any solution from the generalized domain are possible. As an example, the mean and randomly-weighted average combinations of all the incoming frequency-direction queries are implemented, but any user with a function that relies on the  $u(x, y, \omega, \theta)$  solution as an input variable can add theirs to the “User Functions” folder discussed on (3.2.1). The interface will automatically read it on initialization and when it is selected from the drop down menu, the user function will be shown in the main plot axes of Tab 1. As discussed earlier on (3.1.4), the addition of this output opens an endless degree of possibilities to be included in the future by users who may want to implement empiric or experimental functions.

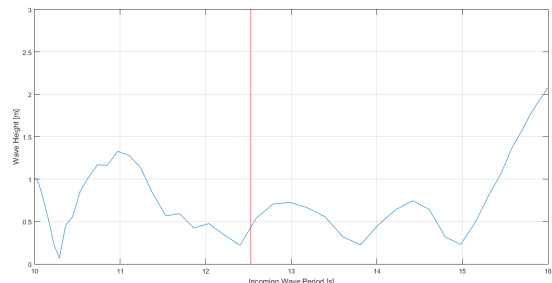
Following the same line of thought, the next tools are able to perform resonance studies in any given spatial point in real-time. Located on the right end side of the layout shown in figure (3.3), the following axes show the distribution of the current tab variable along the parametric dimensions  $\omega$  and  $\theta$  for the user-specified spatial coordinates:



(a) Wave height distribution along the  $\omega$  and  $\theta$  coordinates.



(b) Wave height distribution along the  $\theta$  coordinates.



(c) Wave height distribution along the  $\omega$  coordinates.

Figure 3.12: Example of wave height distribution plots along the incoming frequency and direction parametric coordinates.

These graphs provide very useful information for the identification of the critical wave periods and directions for the selected coordinates, a very important output for resonance studies. These graphs work in conjunction with the input arrow shown in (3.10) by updating the current values in real-time while the arrow is dragged. This allows the user to quickly simulate the desired conditions both in spatial and parametric coordinates, making it much easier to identify the scenarios that could deem navigation unsafe on a certain set of coordinates, for example.

Finally, there are two ways in which the features that require a spacial coordinate specification are triggered. (i) The user can select a single spatial point by clicking on it once to show the active variable's value on that point; (ii) double click on it to additionally show the parametric distributions shown in figure (3.12) for that point; (iii) they could also create a rectangular area selecting an (a) Average, (b) Minimum or (c) Maximum point within, depending on the option selected in the panel located below the main plot axes, on the left:

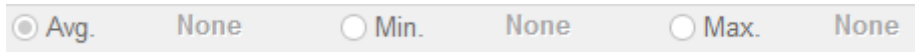


Figure 3.13: Spatial point selector for user-specified region

These outputs are very useful for the assessment of safety of port operations, as many times the wave agitation problem is more pronounced on a reduced area rather than the entire port. Nevertheless, the selection of the full spatial domain in the rectangular area from (iii) could be used in conjunction with the maximum option from (3.13) and the parametric distributions shown in (3.12) to find the worst-possible scenario query, for instance.

## Chapter 4

# Numerical applications

This chapter presents an engineering application of the software developed in this thesis. The aim of the exercise is to demonstrate the applications and functionality of the tool using a realistic setup in which all functionalities described in Chapter 3 are tested.

The first section deals with the preprocessing stage, with an overview of the methodology to obtain the geometry and bathymetry as well as the constraints that have to be fulfilled. Limitations such as maximum mesh size and Finite Element order needed to obtain an acceptable resolution on the solution or the minimum dimensions of the PML area are described. The methodology to obtain the bathymetry file is also explained, with special attention put into the gradient limitations imposed by the MSE on the bottom surface. The choice of a sampling size for the demonstration is also mentioned.

The second section goes into the description of the execution of the Mataro demo on the wave monitoring tool, showing the steps followed to obtain each solution.

### 4.1 Geometries, bathymetries and incident wave data

This section describes the steps taken to create an example that can be loaded into the GUI software. For that, the following steps are explained for the Pasaia harbour, in the northern coast of Spain:

1. **Obtaining a valid geometry:** A compatible port geometry is essential to build the generalized model. In this case, the publicly-available cartography was obtained and treated until all vectors were perfectly aligned to each other.

The contour of the geometry is later divided into different line groups based on their composition (i.e. natural terrain, sand, solid reflecting boundary, PML layer, etc.). The corresponding boundary conditions will later be assigned to these groups when the data is preprocessed.

2. **Determining the PML area:** Seeing that the PML area has to be modelled in

accordance with the specifications mentioned in (2.1.2), i.e. the thickness of the PML area has to be equal to at least 1.5 times the maximum wavelength considered. This forces to start considering the period samples from the beginning of the preprocessing stage.

The national buoy network data suggests that for the Pasaia harbour, the incoming wave directions vary between  $290 - 340^\circ$  while a great majority of periods fall in the  $6 - 14\text{ s}$  range.

Taking into account that the depth on the far-field region equals  $30\text{ m}$ , introducing these values in the dispersion relation from (2.1.1) yields a minimum thickness of  $215\text{ m}$  for the PML region. Seeing that the depth on the far-field region and the PML thickness depend on each other, choosing a safely greater PML thickness is recommended to ensure it's correct behaviour.

In this example, a PML region of  $350\text{ m}$  thickness is chosen to account for the possibilities of longer waves being included:

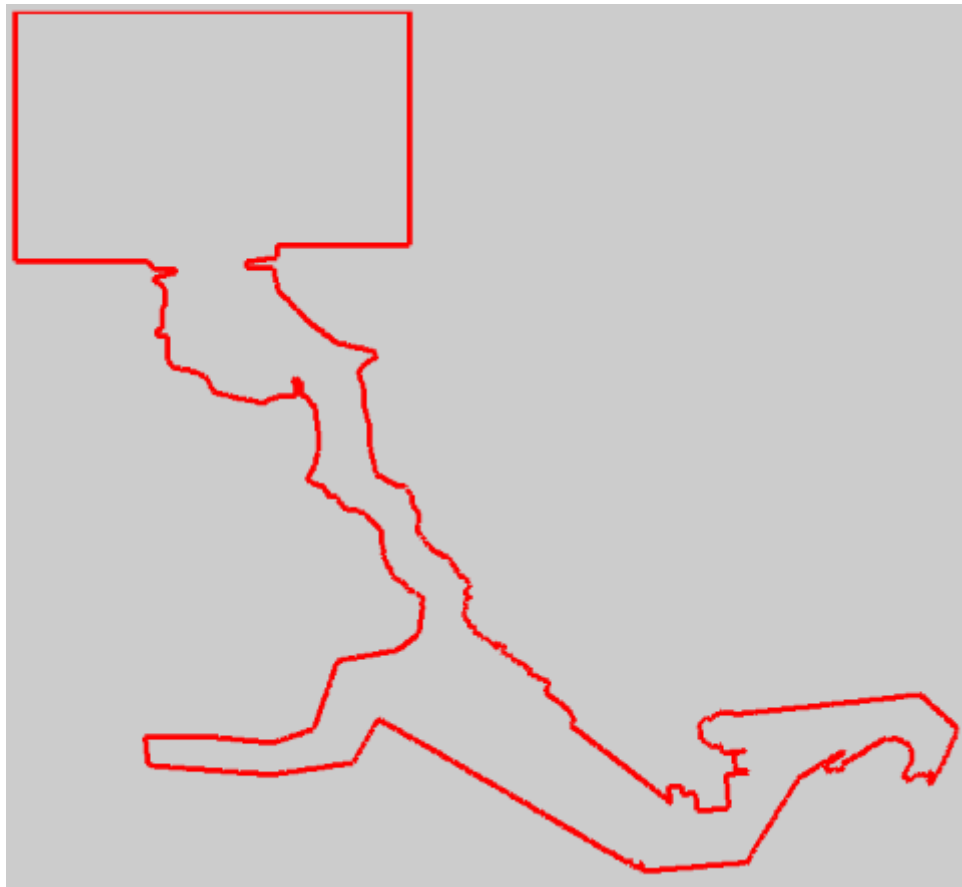


Figure 4.1: Geometric contour of the Pasaia harbour, with the PML included.

3. **Discretization using high-order Finite Elements:** The proposed geometry is modelled using a high-order Finite Element discretization. In this thesis, like in

many other instances of harbour applications, the FEM is applied on the frequential form of the MSE using high-order finite elements ( $p \geq 2$ ). One of the main reasons for which these elements are used is the great reduction on error magnitude when compared to their linear ( $p = 1$ ) counterparts as showed by Giorgiani et al. (2013). This simple solution allows a great error reduction when modelling short waves with medium to high frequencies, specially when modelling complex geometries. Fourth order finite elements used in this thesis allow an accuracy of two significant digits with a low wave resolution, making them an optimal alternative for modelling harbour wave propagation problems with a high number of reflected waves at minimum computational requirements, see Huerta et al. (2013); Sevilla et al. (2013).

For the applications of this thesis, the minimum required resolution is 8 nodes per wavelength, as seen in the thesis by Modesto (2014). The minimum wavelength, according to the dispersion relation (2.1.1), is 137.3 m, which requires  $h < 70$  elements. Here, fourth-order elements of size  $h = 50$  are used to construct the following mesh:

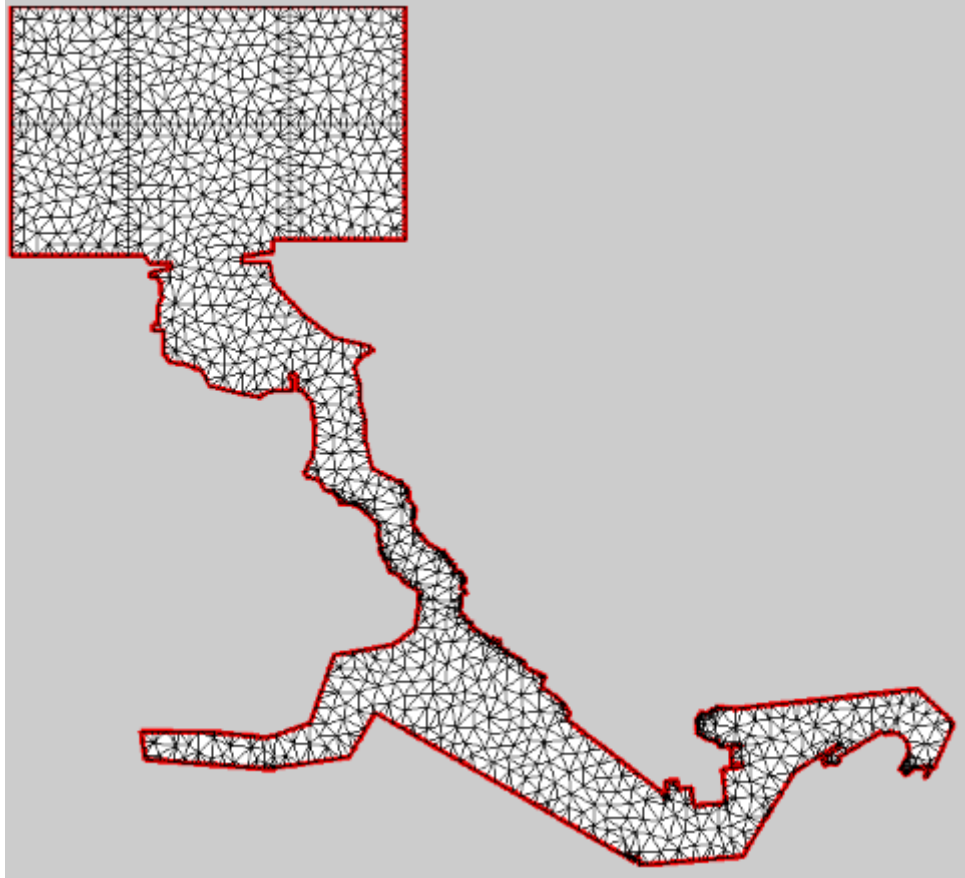


Figure 4.2: High-order Finite Element discretization of the Pasaia harbour.

4. **Obtaining the bathymetry:** While the data used in the previous step to approximate the ocean depth on the far-field region is acceptable, the bathymetric profile in

the harbour domain is far more irregular, so specific bathymetry is needed in order to create the surface of the ocean bottom.

In the numerical example of the Pasaia port, the bathymetry was obtained in a CAD file:

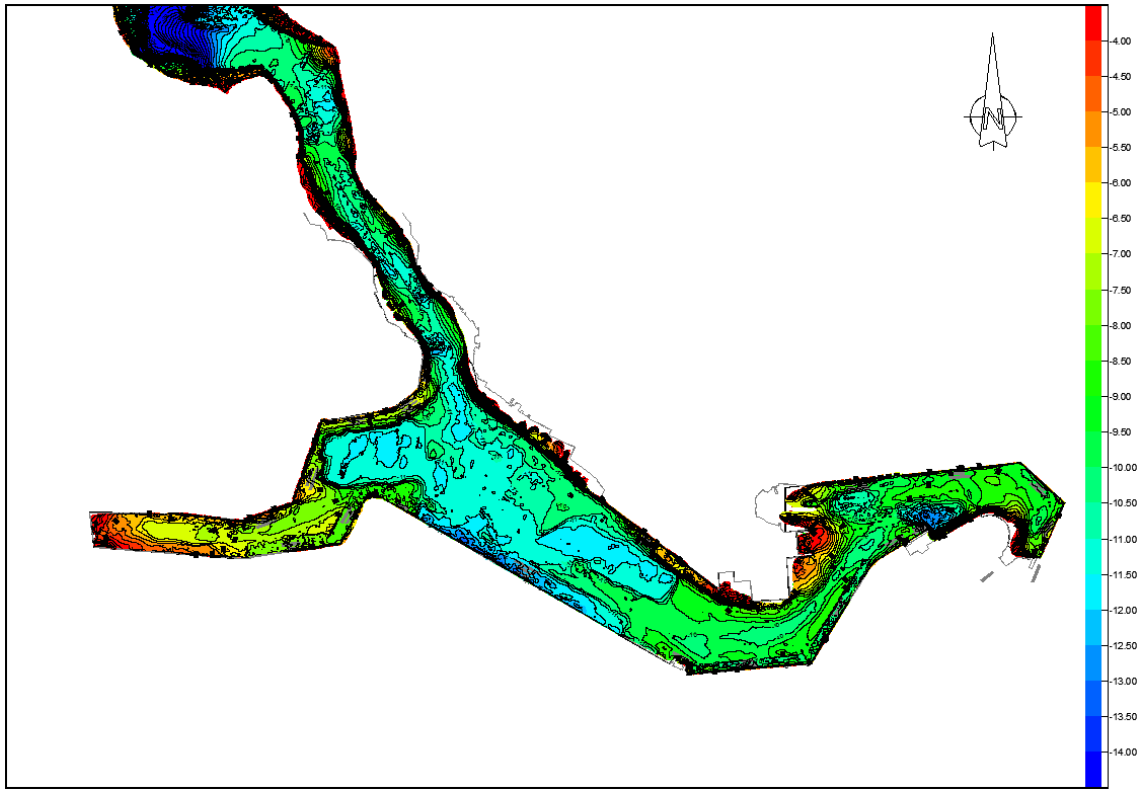


Figure 4.3: Bathymetry drawing for the Pasaia harbour. Plan provided by Pasajes Port Authority

The obtained bathymetry needs to be readable in the MATLAB<sup>©</sup> format, and the CAD file did not contain any point data in XML form, so the following procedure was followed to obtain the bathymetry surface:

- (a) Generate a new script with the Finite Element mesh coordinates as inputs. Generate a *zeroes* vector with the same amount of nodes as the Finite Element mesh, and merge it with the FEM global coordinates matrix.
- (b) Collect several depth samples from the provided map, and take note of them in a MATLAB<sup>©</sup> script file with their respective coordinates from the drawing.
- (c) Search the closest node to each sample point with a ruled connectivity matrix that establishes that only the samples that are closer than a limit distance to a certain node get accounted for. In this example, this measure didn't discard any samples as special care was taken to perform the measurements close to

existing nodes.

- (d) Once sufficient samples are collected, generate an interpolant function that takes into account the distances between the elements to assign the missing depths.
- (e) Evaluate the missing elements through the scattered interpolant to generate a full  $x, y, z$  surface.
- (f) Apply the MSE constraints needed to secure the convergence of the solution, namely that (i) the bathymetry gradient must not be greater than  $1/3$  and (ii) the minimum depth of all the nodes needs to be sufficient to assure a positive gradient matrix, in this case established as  $3.5\text{ m}$ . The modification to the surface when this measures were taken was minimal.
- (g) Export the obtained  $h(x, y)$  surface. In the Pasaia example, the procedure results in the following surface:

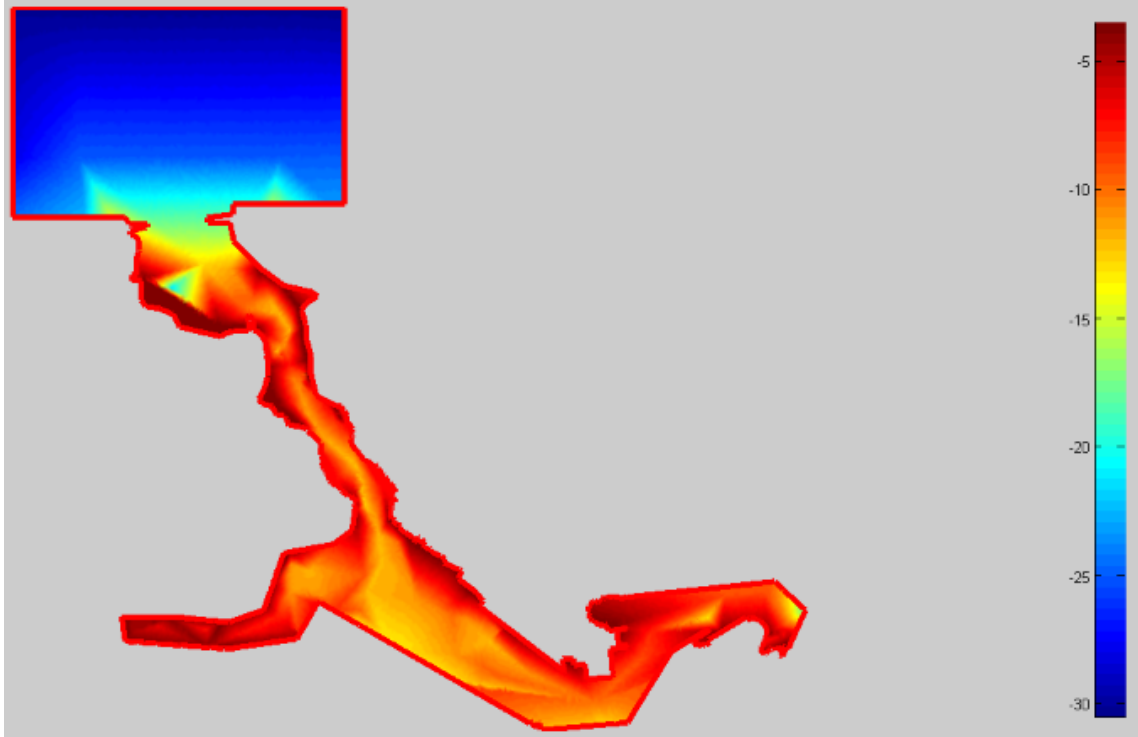


Figure 4.4: Interpolated bottom surface in the Pasaia harbour

5. **Select period and direction ranges for incoming wave parameters:** In this example, the latest yearly histograms of the Pasaia harbour were observed to obtain an input parameter range. The ranges mentioned earlier, when combined, conform more than 86% of incoming wave data.
6. **Assign boundary conditions to contours:** With the geometry and bathymetry

generated, the FE mesh and bottom surface are loaded into a Finite Element Solver to assign boundary conditions to the contours.

7. **Test realistic queries for convergence:** Once all files have been generated, several queries are presented in the FEM solver to test the convergence on the solution and validate the model. Next, an example is shown for a 8 s period, 290° and 1 m incoming amplitude wave:

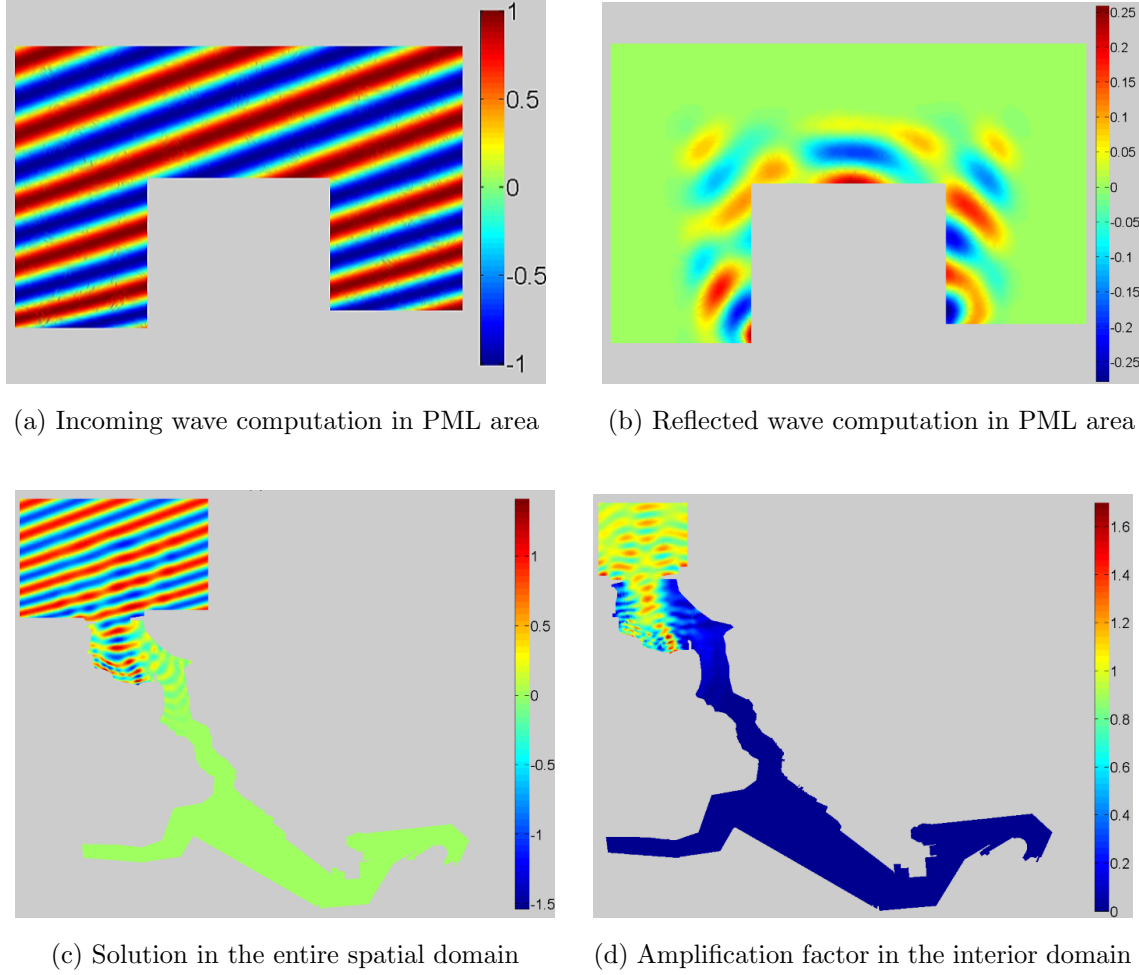


Figure 4.5: Input parameters validation results

8. **Application of the PGD algorithm to generate a generalized solution:**

Once the static input parameters (boundary conditions, bottom, geometry) have been validated, the PGD algorithm is applied to obtain the generalized solution.

## 4.2 A realistic application: Mataro harbour

In the later modelling stage, a previously generated PGD solution is loaded into the GUI described in (3.2) in order to test and demonstrate its capabilities in a realistic situation.

In this case, the chosen scenario is the harbour located in Mataro, Spain. In this section, the sequences outlined in Chapter 3, aiming to obtain the outputs described in (3.1) are implemented.

Once the port is loaded through the location map described in (3.2) and all the variables and functions are assigned, the interactive functionalities are enabled and the data loading algorithm generates the initial plots, showing the following layout:

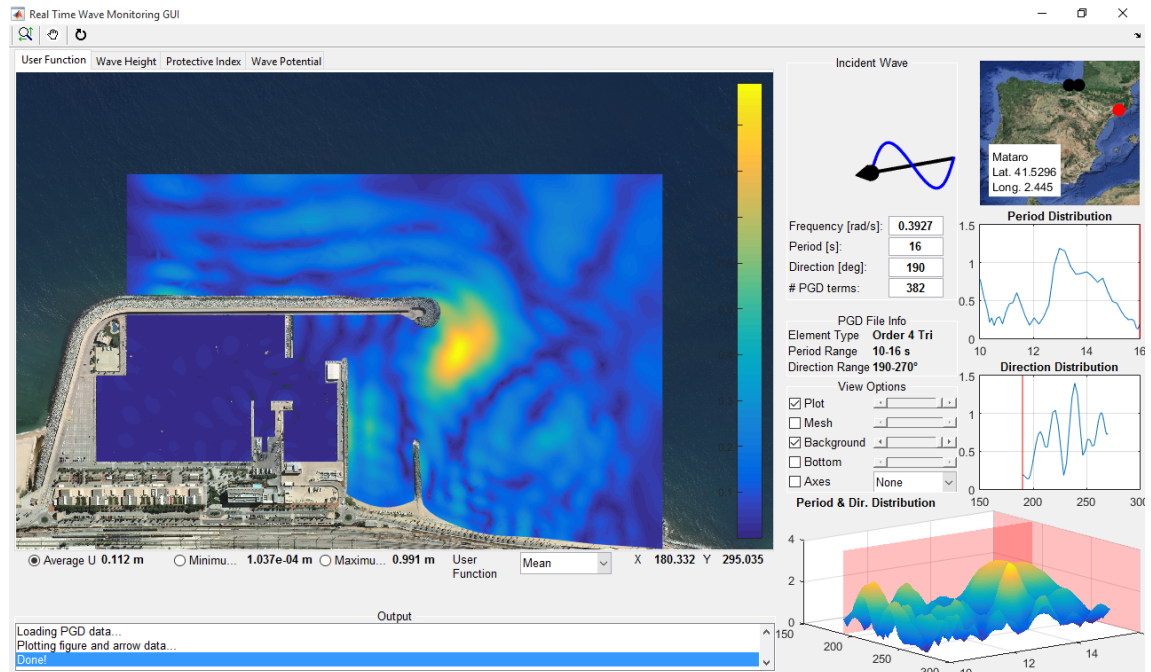


Figure 4.6: Main figure with the Port of Mataro loaded

As can be seen in figure (4.6), the main scalar fields are allocated in tabs on the main plot axes. These are plots for the combined user-specified solution, the wave height solution, the protective index field and finally the wave potential assessment:

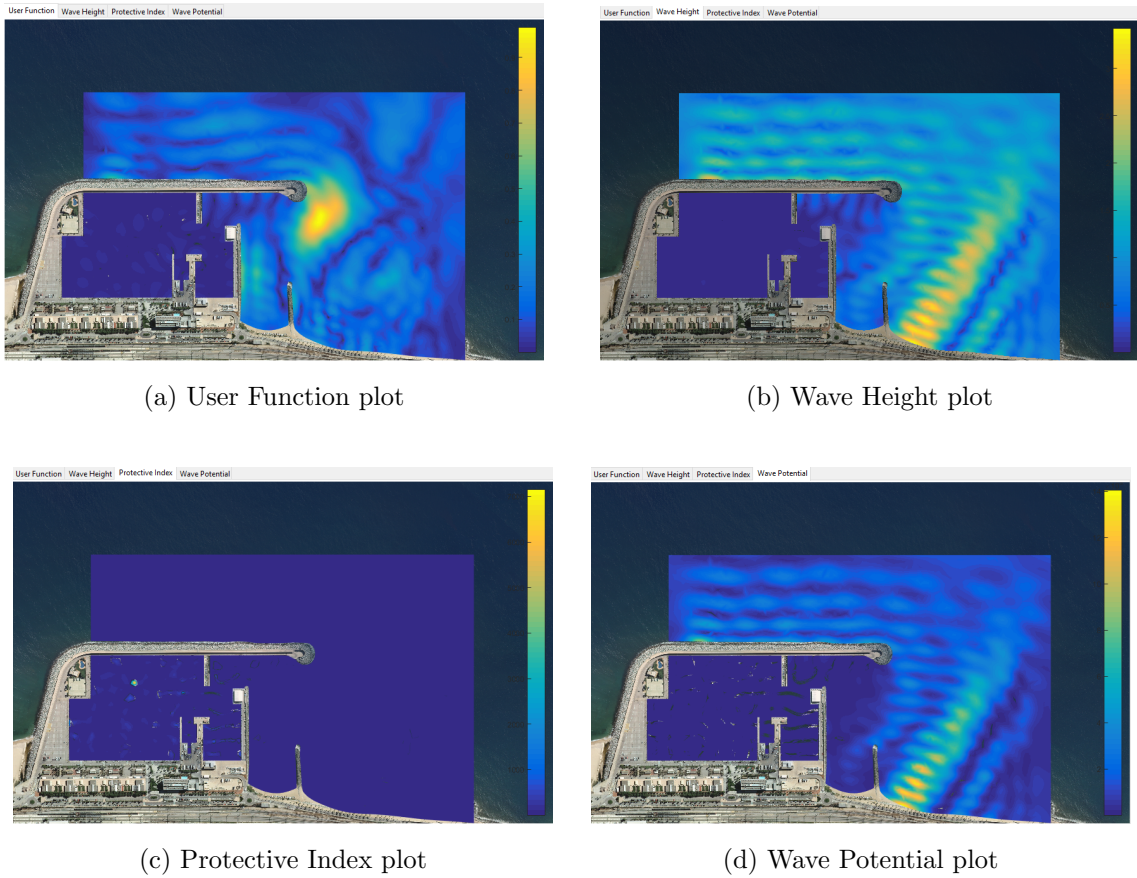


Figure 4.7: Scalar output variable field surfaces

As an extra feature aimed towards increasing the ease of data visualization and the realism of the representation, these plots are 3D surfaces, allowing the combined view of all the layers that can be activated by the “View Options” panel:

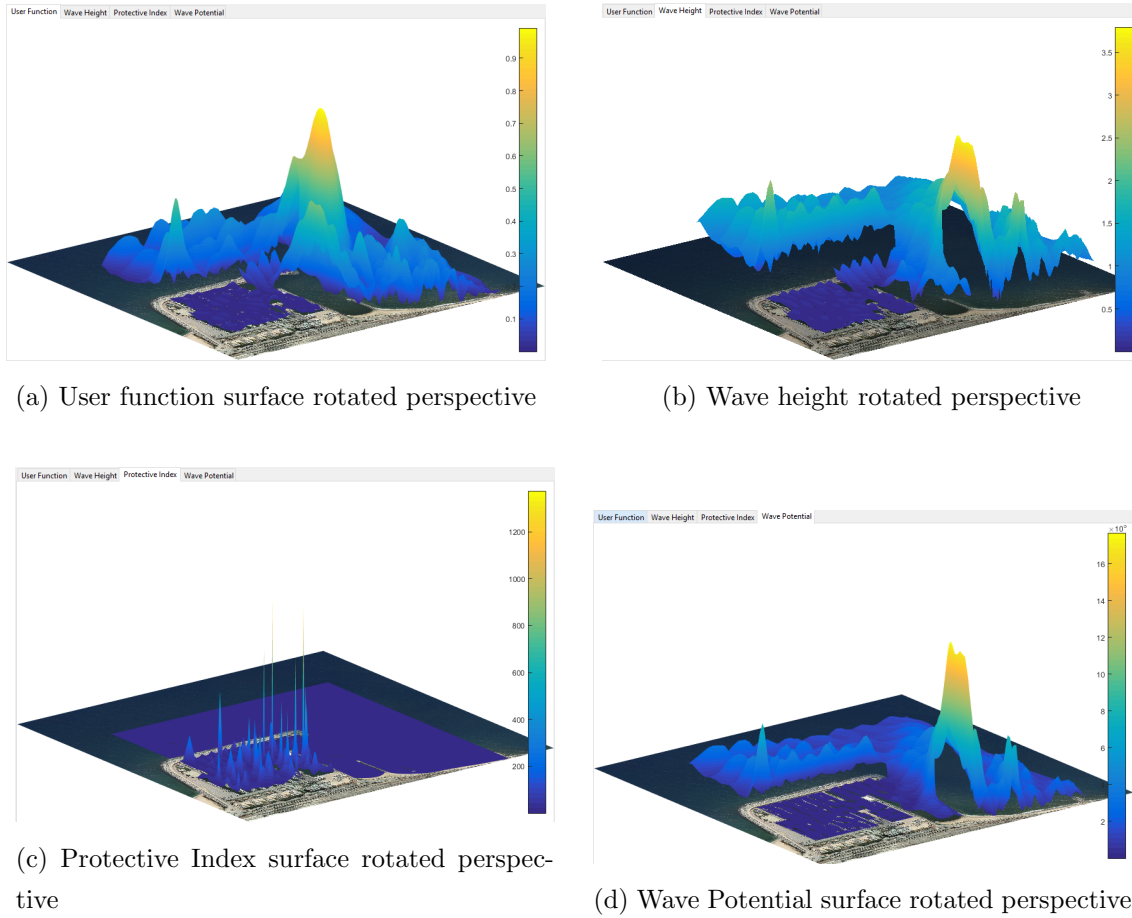


Figure 4.8: Results of 3D surface rotation testing

It is also worth noting that the viewing angle of all four plots is linked in a way that when one of them is rotated, the rest mimic its movement, making it easier to visually relate and compare the different variable fields.

The scalar field plots in (4.7) show the main plots superimposed on the background image extracted from the orthophoto. This feature aids in the visualization of the localized data if, for example, the wave agitation has to be evaluated at the docking point of a certain vessel. Nevertheless, there are several other layers that can be turned on or off via the View Panel:

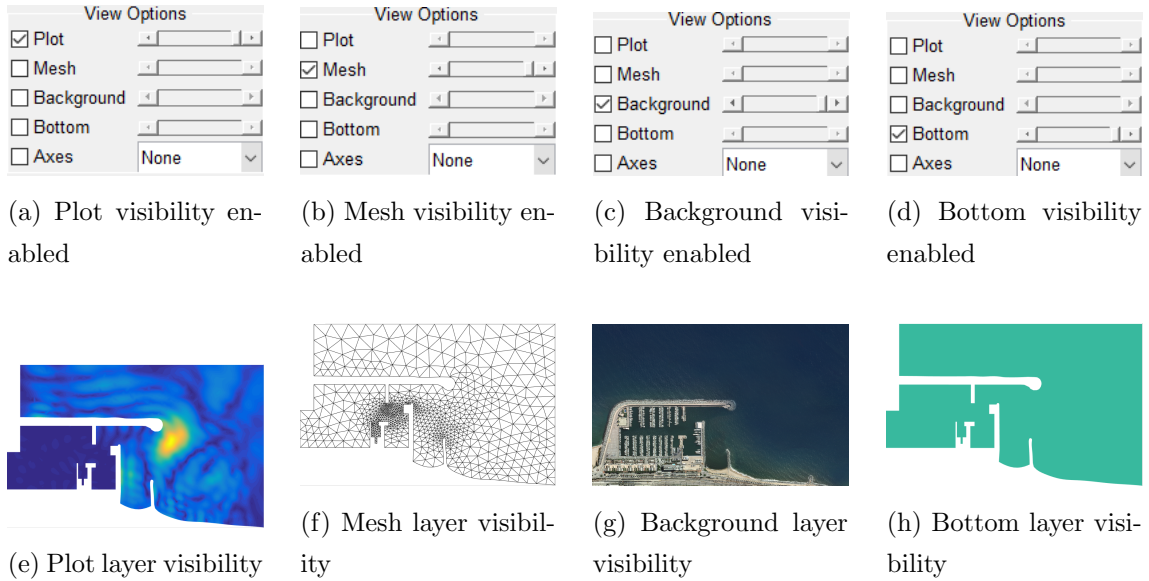


Figure 4.9: Main Plot visibility layer options

One may observe in (4.9) and (4.6) that the background image appears to be bigger than the generated plots. This feature serves two purposes: (i) It aids in the visualization of plots that would otherwise fill most of the space available in the axes, as would have been the case in this example, and (ii), it gives an idea of the dimensions of the PML region, as the edges of the background image are the same ones as the PML region:

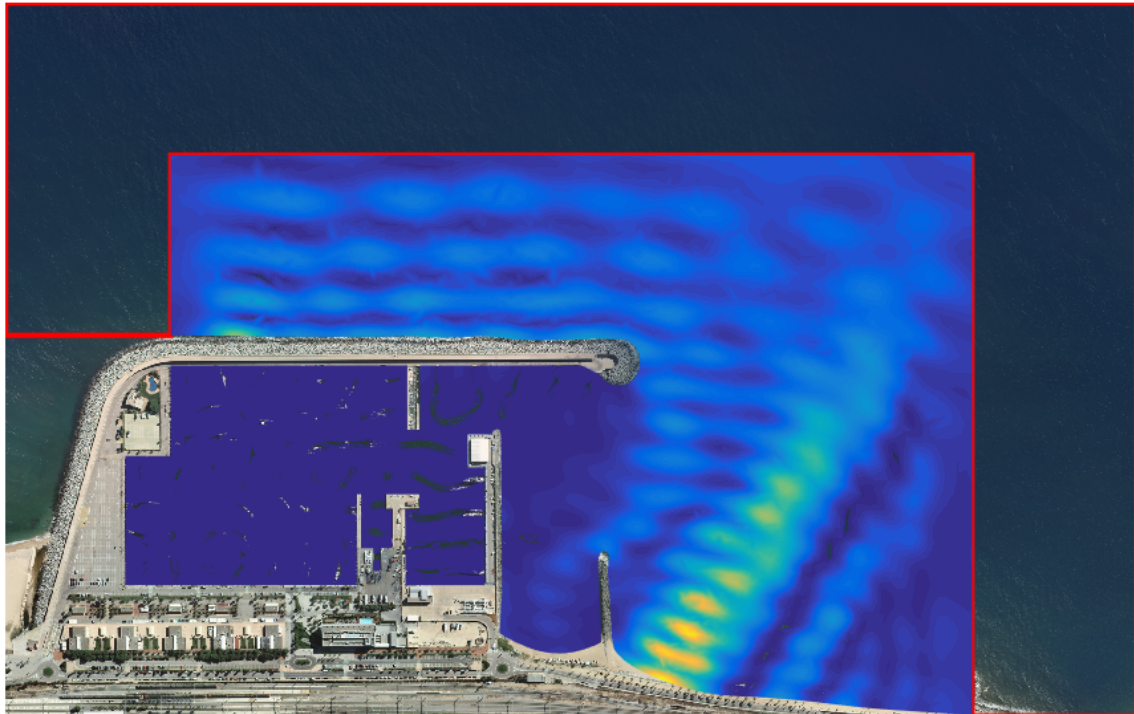


Figure 4.10: Boundary PML region dimensions on background image

Additionally, each one of these layer's transparency can be modified, enabling several options of interest for useful data visualization. For instance, by activating the plot and bottom layers and setting the formers transparency to a low value, it would make it easier to see the effects of the bathymetry on the solution. What follows are several combinations obtained by adjusting the transparency sliders of each element:

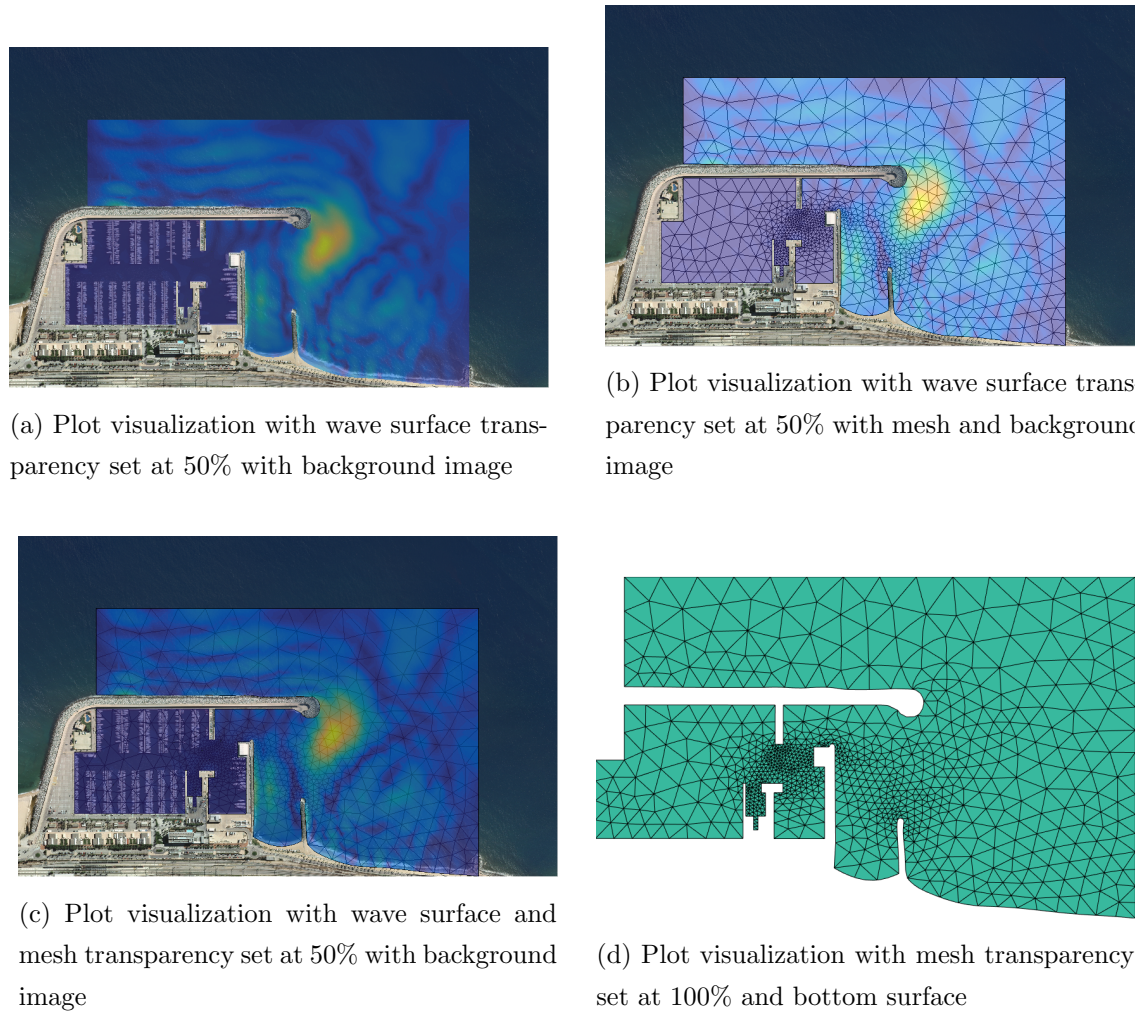


Figure 4.11: Examples of plot visualization transparency combinations

As far as interactive results go, the following functionalities are tested:

- 1. Combined solutions comparison:** The different functions for achieving combined solutions are compared to test if the associated callback generates a new surface every time the selected function is changed.

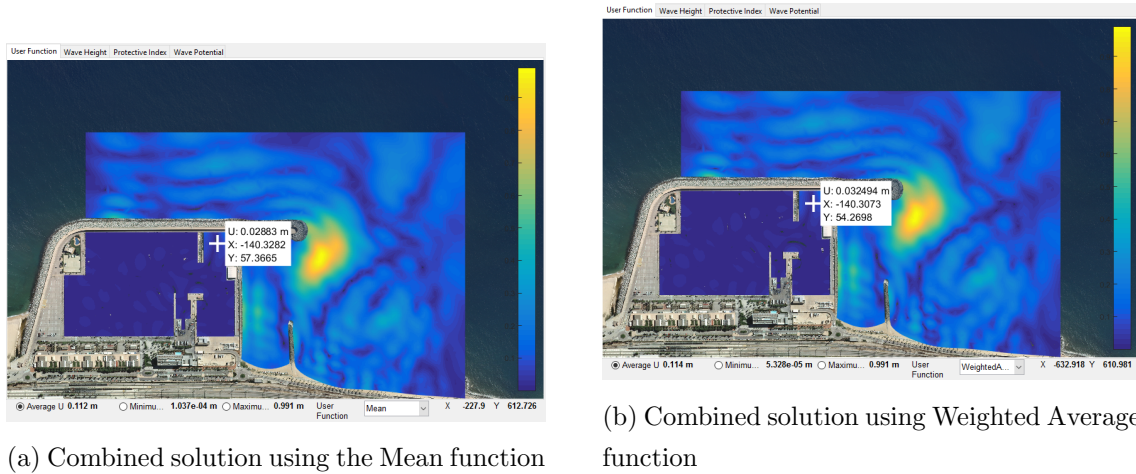
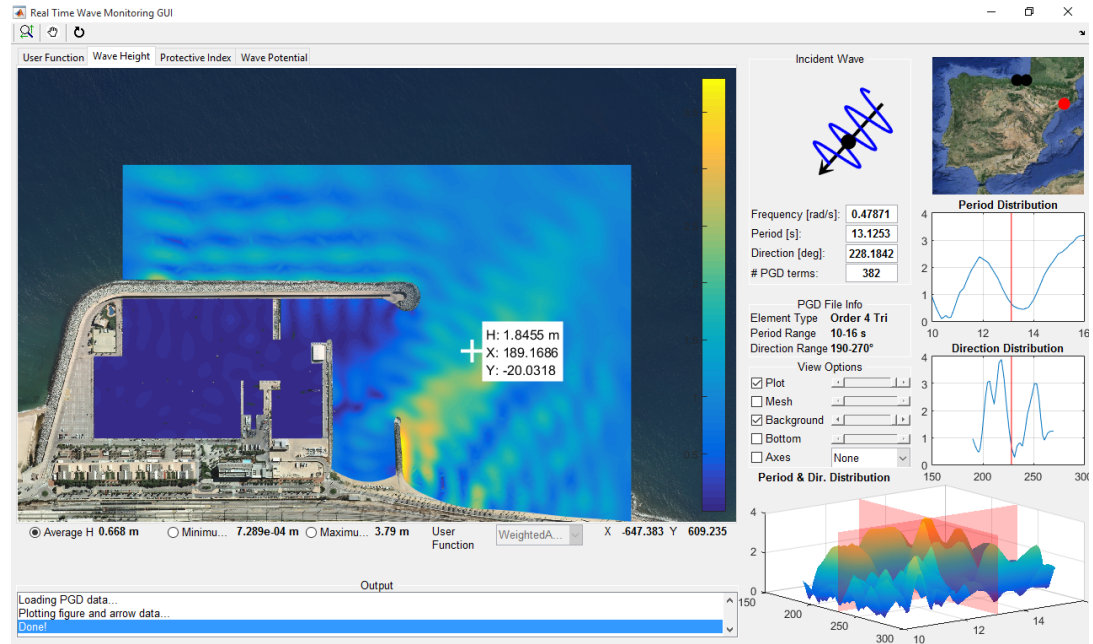


Figure 4.12: Comparison between Mean and Weighted Average combined solutions

Note that the similarity shown between both plots is a result of the weight assignation distribution embedded in on the Weighted Average user function. As a demonstration, weights are randomly assigned in an evenly spaced pattern, with  $\sum w_{ij} = 1$ . Note that the interactive feature to obtain a single localized solution in the spatial domain is tested as well, with positive results.

2. **Resonance studies:** As explained in (3.2.3), double-clicking a spatial point in any surface should yield the parametric distributions of  $\omega$  and  $\theta$  for that selected point. The output of the selected query is shown next:



(a) GUI layout showing parametric distributions on the right for the user-selected point

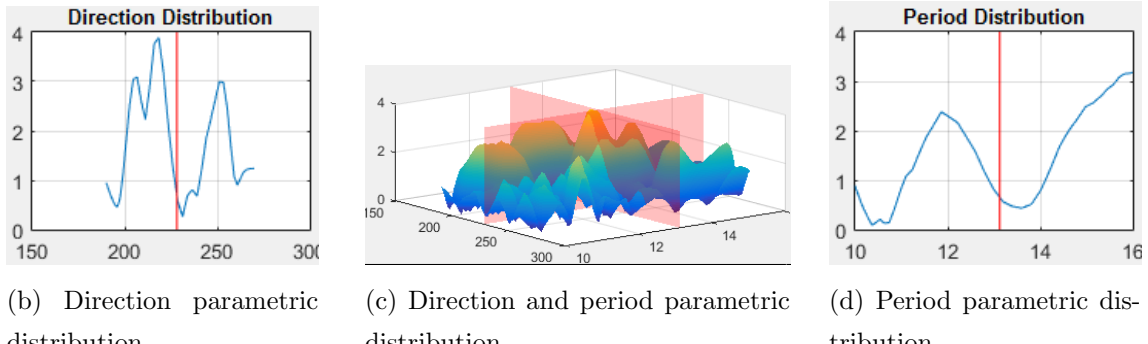


Figure 4.13: Parametric distribution interactive feature testing results

This functionality encountered no errors on its multiple executions, and all the permanent modifications on conflicting variables are avoided, so the implementation is successful for the current example.

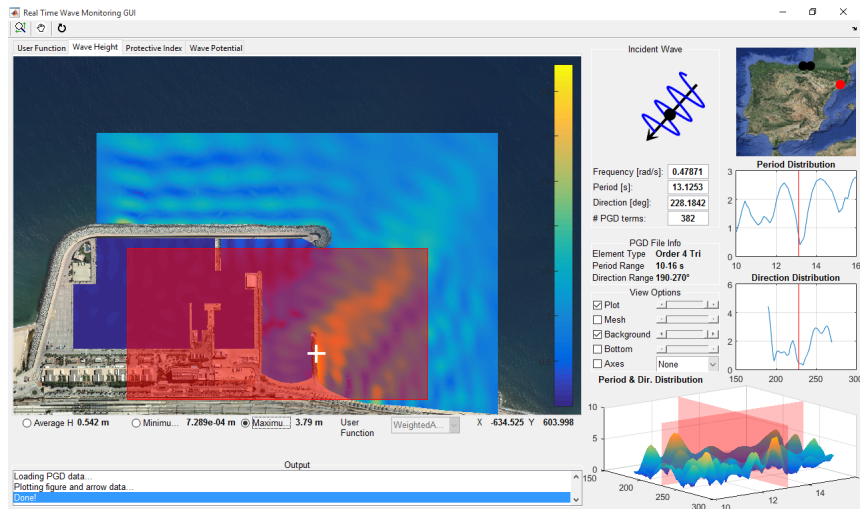
3. **Region selection:** In this section, the same is tested for the selection of a reduced region through user interaction. The added functionality of this feature when compared to the previous one is the possibility to automatically select the current maximum, minimum and average singular spatial points inside the selected region to allow the query of these values in real time. Another possible application is that if the entire spatial domain is selected, the global maximum and minimum points can be obtained, as well as an average point that could be assumed representative of the current-query solution.

4. **Limit heights:** The last interactive output that is tested is the ability to set a limit on the scalar variable that is currently active. This action is triggered by clicking on the desired point in the associated colorbar.

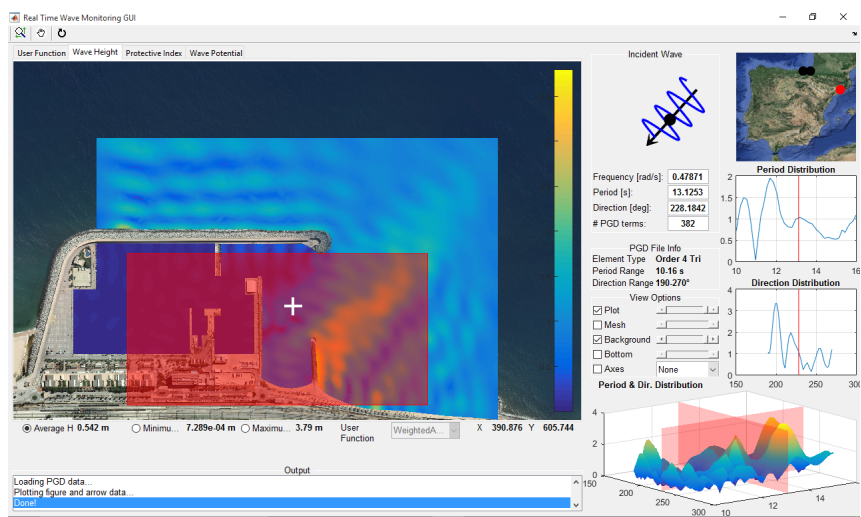
Results for those functionalities are shown on the figures attached on the next two pages.

The results obtained in figure (4.15) show a great interaction and reliability with this function, allowing to quickly assess which zones may be at risk in accordance with the current norms.

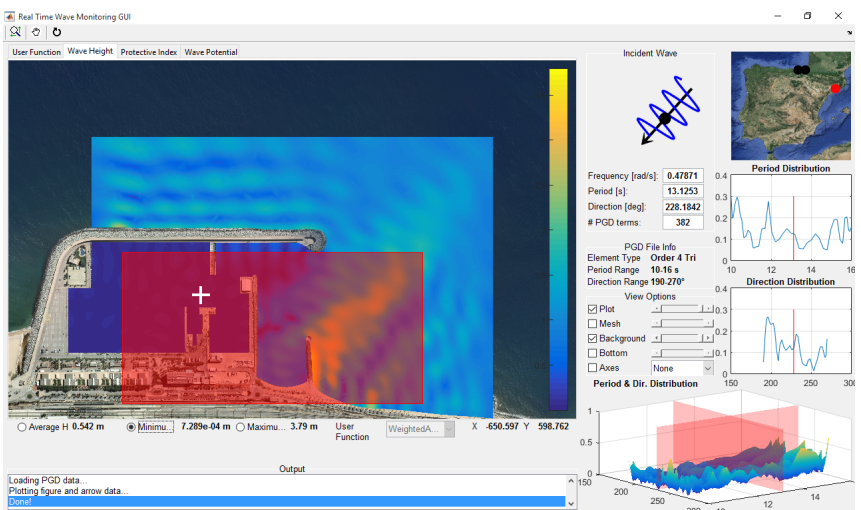
In conclusion, all the outputs presented in (3.1) are achieved without any error and providing the maximum degree of user interaction, in accordance with the main thesis objective defined in (1.3)



(a) Distribution of the maximum wave height point in the selected area

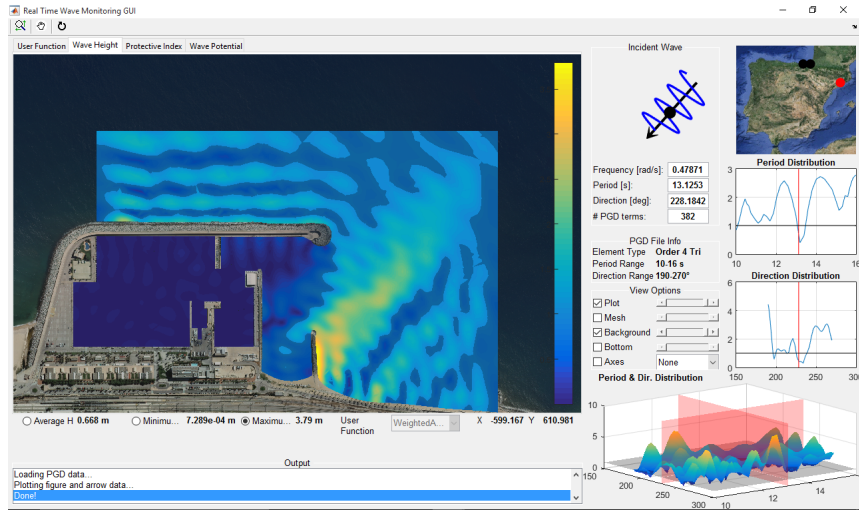


(b) Distribution of one of the average wave height points in the selected area

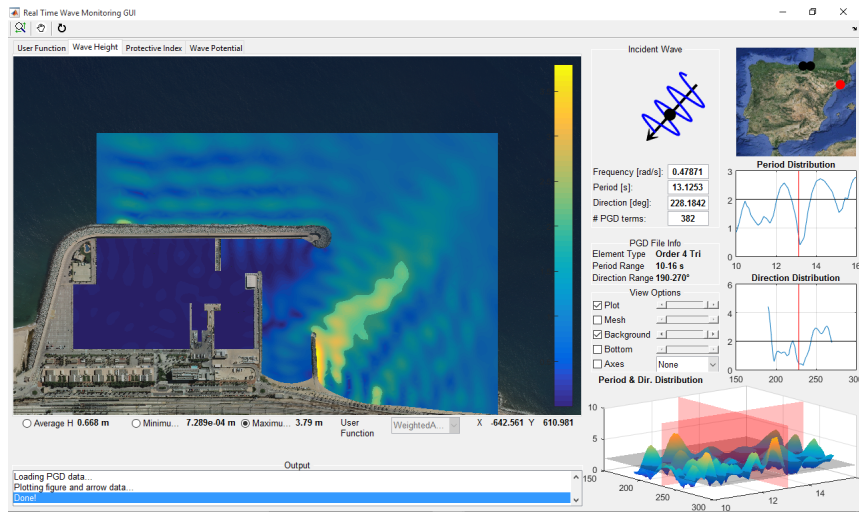


(c) Distribution of the minimum wave height point in the selected area

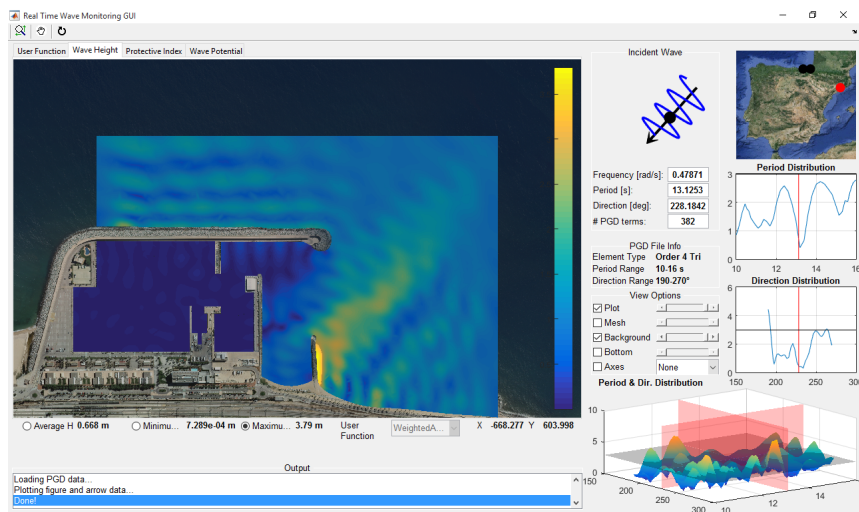
Figure 4.14: Area maximum, average and minimum selections and distributions testing results



(a) Main plot with wave height limit set to 1m



(b) Main plot with wave height limit set to 2m



(c) Main plot with wave height limit set to 3m

Figure 4.15: Limit surface test results

# Chapter 5

## Discussion

### 5.1 Summary and conclusions

The development of a graphical user interface for a real-time wave monitoring tool in elliptic harbour models was proposed in this thesis. For this, first the numerical techniques used to achieve real-time solutions were discussed, with a general overview of the two-stage strategy used to obtain a generalized solution from which the desired multiple-query results could be obtained at a negligible computational cost.

In the second part, most relevant applications were investigated in the initial stage. It was found that most of the outputs of interest that coastal engineers would find useful relied in the capacity to assess wave agitation in real-time through a highly responsive and interactive software. Additional applications found through research included several variables of interest for the practices of coastal engineering and port management. Performing wave propagation models in real-time turned out to be very useful in the quick assessment of the safety of port operations, and the additional output of Protective Index was proposed. Evaluating the options for the energetic output of existing wave currents also has very promising applications in the field of renewable energies, and thus the inclusion of an indicator variable was proposed. Providing expert engineers and users with a way to include their own functions with which solution combinations, or other variables relying on the wave height variable could be obtained promised to greatly increase the applications of the tool. Resonance studies were also considered through the evaluation of the distributions of the wave height variable on the parametric input dimensions. Finally, the applications of the spatially localized solutions were also discussed, as a reduced area or single spatial point selection in which the desired parameters could be evaluated instantly with a high degree of user-friendliness.

In the next part of the thesis the MATLAB<sup>©</sup> GUI development was discussed, with a general overview of the inner workings of the environment in which several files, functions and routines worked together to achieve the best possible implementations of the appli-

cations considered previously. In a later stage, the functionalities of each UI component were presented.

Finally, the developed interface was tested in a realistic application set in the Mataro harbour. For this, first the preprocessing stages needed to model a realistic example were outlined as a guide for future implementations, using the Pasaia harbour as example. Later, each proposed functionality was demonstrated in the Mataro testing environment, delivering the desired results for all queries, with some additional options proving to be very useful in the visualization of the data and the interaction with the solution.

The main goal of this thesis was the development of a real-time wave monitoring tool that included several additional outputs of interest for coastal engineers and port management. This has been accomplished through the fulfilment of the primary and secondary objectives presented in (1.3), following the procedure outlined here. The GUI has been successful in its applications, and further functionalities have been built, with a focus of ease-of-use and intuitive data visualization options.

## 5.2 Future work

This thesis has provided a tool to perform several key evaluations of engineering applications for the harbour wave agitation problem, by analysing and implementing a set of valuable and useful outputs at a negligible computational cost in an intuitive environment. Nevertheless, two research lines suggest promising advancements in the future:

1. **Implementations of wave spectral analysis:** This thesis provides a tool with which realistic wave spectra can be included as an input on the user interface. However, allowing engineers to test the effects of different spectral configurations on the various outputs presented here may have several applications of interest. A tool to generate and evaluate the wave spectral distribution functions prior to the evaluation of the wave agitation problem in harbours could carry promising advancements in the assessment of port safety and design.
2. **Parameter optimization through the increase in PGD dimensionality:** The current form of the PGD adopted in this thesis evaluates the effect of the incoming wave parameters on the solution. Increasing the number of parameters in the PGD to include design variables such as bathymetry configuration or absorbing boundary coefficients could allow to assess the effects of these variables on the solution, and thus enable their optimization or at least have great significance in the design of infrastructure expansion or dredging operations by finding the most favourable parameter values.

# Bibliography

- Adytia, D., Ramdhani, M., and van Groesen, E. (2012). Phase resolved and averaged wave simulations in jakarta harbour. *Coastal Hydrodynamics*, pages 218–223.
- Bellotti, G. (2007). Transient response of harbours to long waves under resonance conditions. *Coast. Eng.*, 54:680–693.
- Berkhoff, J. C. W. (1972). Computation of combined refraction-diffraction. In *Proc. 13th Coastal Engineering Conference*, volume 1, pages 471–490, Vancouver, Canada.
- Berkhoff, J. C. W., Booy, N., and Radder, A. C. (1982). Verification of numerical wave propagation models for simple harmonic linear water waves. *Coast. Eng.*, 6(3):255–279.
- Bettess, P. (1977). Infinite Elements. *Int. J. Numer. Methods Eng.*, 11(1):53–64.
- Chakrabarti, S. K. (1999). Wave interaction with an upright breakwater structure. *Ocean engineering*, 26(10):1003–1021.
- Clément, A., McCullen, P., Falcão, A., Fiorentino, A., Gardner, F., Hammarlund, K., Lemonis, G., Lewis, T., Nielsen, K., Petroncini, S., et al. (2002). Wave energy in europe: current status and perspectives. *Renewable and sustainable energy reviews*, 6(5):405–431.
- Cox, A. T. and Cardone, V. J. (2002). 20 years of operational forecasting at oceanweather. In *7th International Workshop on Wave Hindcasting and Forecasting October*, pages 21–25.
- Demirbilek, Z., Xu, B., and Panchang, V. (1996). Uncertainties in the validation of harbor wave models. *Coastal Engineering Proceedings*, 1(25).
- Diaz-Hernandez, G., Mendez, F. J., Losada, I. J., Camus, P., and Medina, R. (2015). A nearshore long-term infragravity wave analysis for open harbours. *Coastal Engineering*, 97:78–90.
- Giorgiani, G., Modesto, D., Fernández-Méndez, S., and Huerta, A. (2013). High-order continuous and discontinuous Galerkin methods for wave problems. *Int. J. Numer. Methods Fluids*, 73(10):883–903.

- González-Marco, D., Sierra, J. P., de Ybarra, O. F., and Sánchez-Arcilla, A. (2008). Implications of long waves in harbor management: The gijón port case study. *Ocean & Coastal Management*, 51(2):180–201.
- Guerrini, M., Bellotti, G., Fan, Y., and Franco, L. (2014). Numerical modelling of long waves amplification at marina di carrara harbour. *Applied Ocean Research*, 48:322–330.
- Huerta, A., Angeloski, A., Roca, X., and Peraire, J. (2013). Efficiency of high-order elements for continuous and discontinuous Galerkin methods. *Int. J. Numer. Methods Eng.*, 96(9):529–560.
- Iglesias, G., López, M., Carballo, R., Castro, A., Fraguela, J. A., and Frigaard, P. (2009). Wave energy potential in galicia (nw spain). *Renewable Energy*, 34(11):2323–2333.
- Kirby, J. T. (1984). Note on linear surface wave-current interaction over slowly varying topography. *J. Geophys. Res.*, 89(NC1):745–747.
- Kofoed-Hansen, H., Kerper, D. R., Sørensen, O. R., and Kirkegaard, J. (2005). Simulation of long wave agitation in ports and harbours using a time-domain boussinesq model. In *Proceedings of Fifth International Symposium on Ocean Wave Measurement and Analysis-Waves. Madrid, Spain*.
- Lee, J.-J., Lai, C.-P., and Li, Y. (1998). Application of computer modeling for harbor resonance studies of long beach & los angeles harbor basins. *Coastal Engineering Proceedings*, 1(26).
- LI, R., ZHANG, S., and ZHANG, Y. (2005). Comparison between characteristics of mild slope equations and boussinesq equations. *Acta oceanologica sinica*, 24(4):131–137.
- Liu, P. L.-F. and Losada, I. J. (2002). Wave propagation modeling in coastal engineering. *J. Hydraul. Res.*, 40(3):229–240.
- Losada, I. J., González-Ondina, J. M., Díaz-Hernández, G., and González, E. M. (2008). Numerical modeling of nonlinear resonance of semi-enclosed water bodies: Description and experimental validation. *Coast. Eng.*, 55(1):21–34.
- Massel, S. R. (1993). Extended refraction-diffraction equation for surface waves. *Coast. Eng.*, 19(1-2):97–126.
- Masson, D. and Chandler, P. (1993). Wave groups: a closer look at spectral methods. *Coastal Engineering*, 20(3):249–275.
- Michler, C., Demkowicz, L., Kurtz, J., and Pardo, D. (2007). Improving the performance of perfectly matched layers by means of hp-adaptivity. *Numer. Meth. Part. Differ. Equ.*, 23(4):832–858.

- Modesto, D. (2014). *Real-time wave monitoring for elliptic harbor models: an a priori reduced order approach*. PhD thesis, Technical University of Catalonia, Spain.
- Mørk, G., Barstow, S., Kabuth, A., and Pontes, M. T. (2010). Assessing the global wave energy potential. In *Proc. of 29th International Conference on Ocean, Offshore and Arctic Engineering, ASME, paper*, volume 20473.
- Muir, L. R. and El-Shaarawi, A. (1986). On the calculation of extreme wave heights: a review. *Ocean Engineering*, 13(1):93–118.
- Panchang, V., Chen, W., Xu, B., Schlenker, K., Demirbilek, Z., and Okihiro, M. (2000). Exterior bathymetric effects in elliptic harbor wave models. *J. Waterw. Port Coast. Ocean Eng.*, 126(2):71–78.
- Rodriguez, G., Soares, C. G., Pacheco, M., and Pérez-Martell, E. (2002). Wave height distribution in mixed sea states. *Journal of Offshore Mechanics and Arctic Engineering*, 124(1):34–40.
- Sevilla, R., Hassan, O., and Morgan, K. (2013). An analysis of the performance of a high-order stabilised finite element method for simulating compressible flows. *Comput. Methods Appl. Mech. Eng.*, 253(0):15–27.
- Soares, C. G. and Carvalho, A. (2003). Probability distributions of wave heights and periods in measured combined sea-states from the portuguese coast. *Journal of Offshore Mechanics and Arctic Engineering*, 125(3):198–204.
- Srokosz, M. and Challenor, P. (1987). Joint distributions of wave height and period: A critical comparison. *Ocean Engineering*, 14(4):295–311.
- Thomas, T. J. and Dwarakish, G. (2015). Numerical wave modelling—a review. *Aquatic Procedia*, 4:443–448.
- Tsay, T.-K. and Liu, P. L.-F. (1983). A finite element model for wave refraction and diffraction. *Appl. Ocean Res.*, 5(1):30–37.
- Vela, J., Pérez, B., González, M., Otero, L., Olabarrieta, M., Canals, M., and Casamor, J. (2014). Tsunami resonance in Palma bay and harbor, Majorca island, as induced by the 2003 Western Mediterranean earthquake. *J. Geol.*, 122(2):165–182.
- Wood, N. J. and Good, J. W. (2004). Vulnerability of port and harbor communities to earthquake and tsunami hazards: The use of gis in community hazard planning. *Coastal Management*, 32(3):243–269.